2015

Analysis of spatio-temporal changes in annual and seasonal precipitation variability in South America-Chile and related ocean–atmosphere circulation patterns

Rodrigo Valdés- Pineda
University of Arizona, Tucson, rvaldes@email.arizona.edu

Juan B. Valdés
University of Arizona, Tucson

Henry F. Diaz
University of Colorado, Boulder

Roberto Pizarro- Tapia
University of Talca, Chile

INTERNATIONAL JOURNAL OF CLIMATOLOGY
Int. J. Climatol. (2015)
Published online in Wiley Online Library
(wileyonlinelibrary.com) DOI: 10.1002/joc.4532

RMetS
Royal Meteorological Society

Analysis of spatio-temporal changes in annual and seasonal precipitation variability in South America-Chile and related ocean–atmosphere circulation patterns

Rodrigo Valdés-Pineda,[a,b]* Juan B. Valdés,[a] Henry F. Diaz[c,d] and Roberto Pizarro-Tapia[b]

[a] *Department of Hydrology and Water Resources, University of Arizona, Tucson, AZ, USA*
[b] *Technological Center of Environmental Hydrology, University of Talca, Chile*
[c] *Cooperative Institute for Research in Environmental Sciences (CIRES), University of Colorado, Boulder, CO, USA*
[d] *National Oceanic and Atmospheric Administration (NOAA), Boulder, CO, USA*

ABSTRACT: Establishing relationships between coupled ocean–atmospheric patterns and precipitation accumulation is important to describe and predict spatio-temporal variability on annual or seasonal scales, and also to evaluate how this variability is influenced by global warming. The objective of this study was to examine the leading modes of interannual and seasonal (summer, autumn, winter, and spring) precipitation variability in South America-Chile, and their significant relationship to seasonally aggregated gridded data and climatic indices. Applying exhaustive data quality control measures to data from 238 rain gauges with different lengths of records between 1893 and 2013, a new data set was created with the objective of obtaining reliable records for further analysis. A comprehensive analysis through empirical orthogonal functions (EOF) allowed for determination of the leading modes of annual and seasonal precipitation and their main spatial patterns for the whole country. The percentage of explained variance in the relationship between seasonally aggregated indices and the leading modes of precipitation confirmed that most of the interannual and winter precipitation variability in Chile is linked to the seasonal aggregation of El Nino Southern Oscillation (ENSO). The leading modes of summer, autumn, and spring precipitation were mostly linked to seasonal aggregations of the Madden and Julian Oscillation (MJO), and the Antarctic Oscillation (AAO).

KEY WORDS precipitation in Chile; annual and seasonal variability; EOF analysis; climate indices

Received 3 December 2014; Revised 12 September 2015; Accepted 14 September 2015

1. Introduction

Rainfall variability can be defined as the degree to which rainfall amounts vary spatially or temporally over a wide range of scales. Knowledge and understanding of such variability may lead to improve risk management practices in agricultural, industrial, and other human activities (Meinke *et al.*, 2005; Trenberth *et al.*, 2007; IPCC, 2012). This information can also help in predicting changes in the precipitation patterns associated with global warming (Hartmann *et al.*, 2013).

Seasonal variability over the South American continent is evident in long-term monthly means of precipitation accumulation (e.g. Marengo *et al.*, 2001; Garreaud *et al.*, 2009; Bombardi *et al.*, 2014). During the austral winter, precipitation accumulation reveals numerous maxima located in the tropical regions along the east–west-oriented intertropical convergence zone (ITCZ) (Andrews *et al.*, 2003; Marshall *et al.*, 2014), while the central part of the continent experiences its dry season (Garreaud *et al.*, 2009). During the austral summer, an extensive area of heavy precipitation extends from the southern half of the Amazon Basin to northern Argentina. This southward shift of convection returns gradually to northern South America during austral fall (Garreaud *et al.*, 2009). This migration, defined by scientists as the South American monsoon system (SAMS), is considered the most important climatic feature in tropical and subtropical regions of South America (Zhou and Lau, 1998; Vera *et al.*, 2006; Marengo *et al.*, 2012; Carvalho *et al.*, 2012). The extratropical regions of South America exhibit a marked zonal asymmetry, with wetter conditions to the west of the Andes cordillera. In contrast, forced subsidence over the eastern side of the Andes produces very dry conditions in Argentina's Patagonia (Garreaud *et al.*, 2009). Mid-latitude storms tend to drift eastward along latitudinal bands known as storm tracks (Garreaud and Aceituno, 2007). South of 40°S, low-level westerlies prevail year-round over the oceans and the continent, in connection with a mean poleward decrease in sea level pressure (SLP) and sea surface temperature (SST) (Figure 1). The mid-latitude westerlies extend through the entire troposphere, reaching a maximum speed (subtropical jet stream) in the upper troposphere (Figure 1(b) and (d)). This jet

* Correspondence to: R. Valdés-Pineda, Department of Hydrology and Water Resources, University of Arizona, J W Harshbarger Bldg, 1133 James E. Rogers Way #122, Tucson, AZ 85721, USA. E-mail: rvaldes@email.arizona.edu

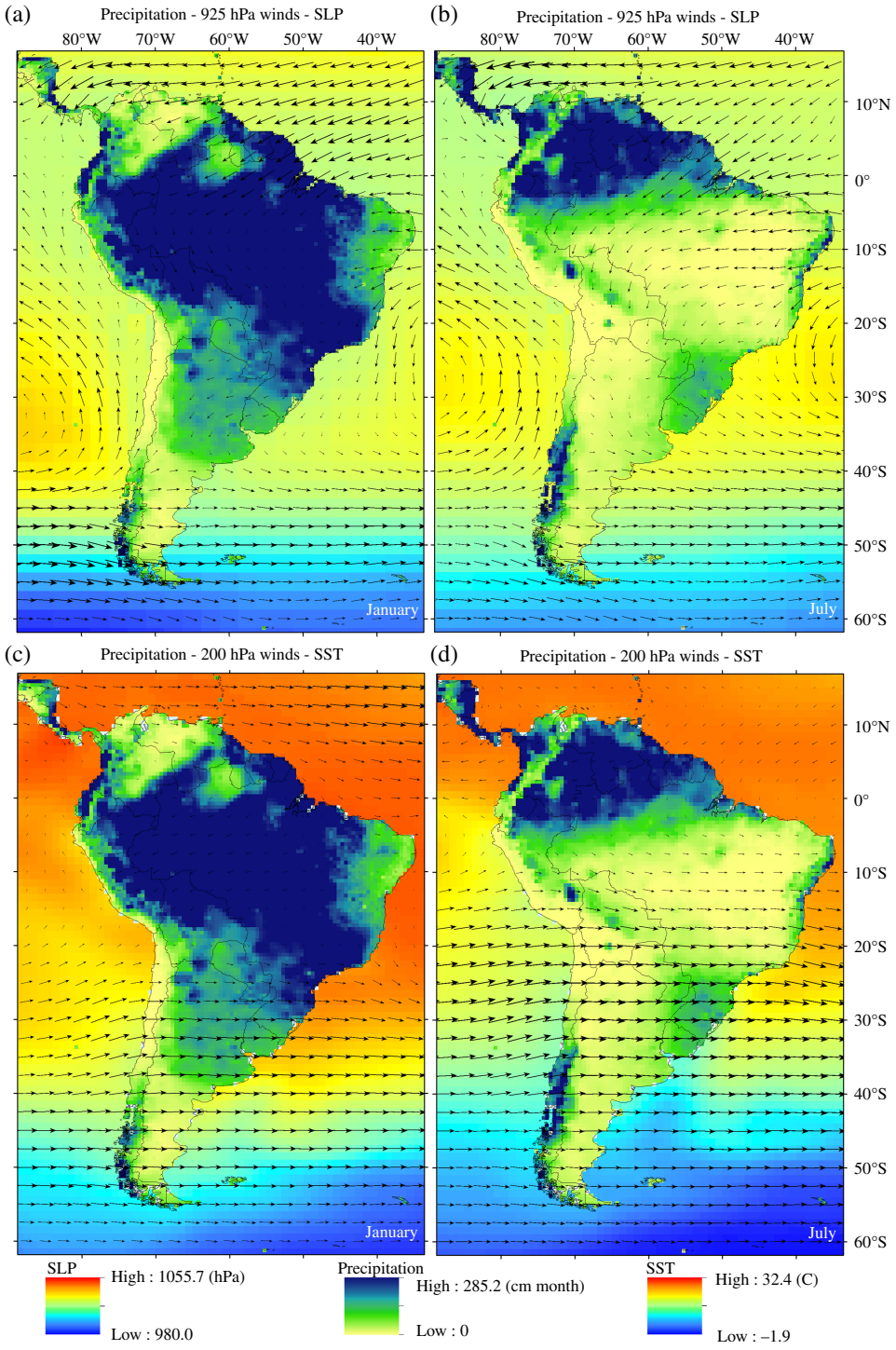

Figure 1. Delaware long-term mean precipitation for July and January (1981–2010). Upper maps are superimposed with low-level wind vectors (925 hPa, about 1000 m.a.s.l.) and SLP obtained from NCEP/NCAR Reanalysis. Lower maps are superimposed with streamlines (200 hPa, about 12 000 m.a.s.l.) and SST obtained from NCEP/NCAR Reanalysis.

stream is commonly located between the 400 and 100 hPa levels (7–16 km) (Archer and Caldeira, 2008). During the austral winter, the low-level westerlies and the subtropical jet stream move equatorward. Thus, the area affected by mid-latitude precipitation over western South America expands up to about 30°S in austral winter (Figure 1(b) and (d)), and then retracts to the south of 40°S during austral summer (Figure 1(a) and (c)) (Garreaud *et al.*, 2009).

All these climate features of South America play an important role in modulating the climate patterns in Chile. However, the exceptional topographic variation of the country is other crucial factor to take into account when analysing precipitation variability at different temporal scales. For instance, Chile is narrow (ranging from 90 to 445 km), constrained between the Andes and the coast of Pacific Ocean. In addition, its north–south extent, of

more than 4000 km, contributes to a wide variety of climates. The overall pattern shows that annual precipitation accumulation increases southward as well as windward of the Andes due to orographic effect (Garreaud *et al.*, 2009; Pizarro *et al.*, 2012; Quintana and Aceituno, 2012; Valdés-Pineda *et al.*, 2014; Viale and Garreaud, 2015). However, the activity of the El Nino Southern Oscillation (ENSO), the Pacific Decadal Oscillation (PDO), the Antarctic Oscillation (AAO), and the Madden and Julian Oscillation (MJO) (for details, see Appendix S1, Supporting Information), in connection with the proximity to the South East Pacific Anticyclone (SEPA), the Antarctic Circumpolar Current (ACC), and the cold Humboldt Current (Peruvian Current), creates three general annual precipitation cycles in the country, northern, central, and austral (Rutllant and Fuenzalida, 1991; Vargas *et al.*, 2000; Montecinos and Aceituno, 2003; Carrasco, 2006; Garreaud *et al.*, 2009; Barrett *et al.*, 2012; Quintana and Aceituno, 2012; Villalba *et al.*, 2012; Ancapichún and Garcés-Vargas, 2015). In northern Chile (17°30′–30°S), an extremely hyper-arid climate is observed in the Central Valley (below 2300 m.a.s.l.), characterized by a lack of precipitation (less than 1 mm year^{-1}), very low humidity, and the general absence of clouds (Houston, 2006). During the austral summer, wet episodes tend to occur throughout the Western Cordillera and Altiplano (plateaus with elevations greater than 3000 m). This occurs because strong upper-level easterly winds enhance moisture transport from Amazonia, creating saturation during uplift within deep convection cells (Garreaud *et al.*, 2003). This climate feature is popularly known as 'Bolivian Winter'; however, as previously mentioned, it is scientifically identified as the SAMS. The character of SAMS produces a rain shadow effect over the Western Cordillera and Atacama Desert, which is evidences by the rapid decline of mean annual precipitation from over 300 mm year^{-1} at 5000 m.a.s.l. to less than 20 mm year^{-1} at 2300 m.a.s.l. (see also Vuille *et al.*, 1998; Garreaud, 1999; Vuille, 1999; Garreaud, 2000; Garreaud and Aceituno, 2001; Garreaud *et al.*, 2003; Houston and Hartley, 2003; Houston, 2006; Minvielle and Garreaud, 2011).

Central Chile (30°–40°S) has a well-defined annual cycle characterized by a peak of precipitation accumulation in the austral winter, and much lower values in the austral summer (Valdés-Pineda *et al.*, 2015). This strong seasonality of precipitation results from the winter retreat of SEPA, which allows stronger low-level westerlies carrying frontal systems to the continent (for details, see Montecinos and Aceituno, 2003; Falvey and Garreaud, 2007). The annual accumulation increases southward from around 100 mm at 30°S to nearly 2000 mm at 40°S (Quintana and Aceituno, 2012), and is concentrated from May to September (Montecinos and Aceituno, 2003). Precipitation amounts also increase eastward due to the orographic effect (i.e. an altitudinal increase); in fact, the windward slopes of the Andes between 32° and 35°S can experience up to twice the precipitation observed over the western lowlands (Falvey and Garreaud, 2007; Viale and Garreaud, 2015).

In the austral region (40°–56°30′S), frontal cyclones drifting eastward along the oceanic storm tracks are responsible for most of the precipitation and day-to-day weather variations (Quintana and Aceituno, 2012; Garreaud *et al.*, 2014). In general, precipitation exhibits a marked zonal asymmetry, with very wet (dry) conditions to the west (east) of the Andes cordillera (Garreaud *et al.*, 2009). This pattern is consistent with strong westerlies throughout the year, which result in precipitation reaching more than 4000 mm year^{-1} and occurring in all four seasons along the western Andes (Carrasco *et al.*, 2002; Villarroel, 2013), while producing a dramatic decrease to about 200 mm year^{-1} in Argentina's Patagonia due to rain shadow east of the Andes (Aravena and Luckman, 2009; Garreaud *et al.*, 2009).

Although there is already in-depth knowledge about the ocean–atmospheric processes affecting Chile, this study aims to detect how the leading modes of annual and seasonal precipitation (DJF for summer, MAM for spring, JJA for winter, and SON for autumn) are related to gridded data and different seasonally aggregated climate indices, i.e. the Southern Oscillation Index (SOI), the bivariate ENSO index (BEST), multivariate ENSO index (MEI), AAO, PDO, and MJO, among others. Specifically, this study examines *how much interannual and seasonal variability can be explained by the leading modes of precipitation accumulation, whether any significant spatial patterns can be identified, and what seasonally aggregated climate indices can better explain the variability of the annual and seasonal leading modes of precipitation.* The main aspects of the methodology, results, and discussion are in the main text, and further details about the methods and results of this study are presented in the Appendix S1.

2. Methodology

2.1. Study area, data set, and quality control

Continental Chile is located on the East Pacific Coast of South America between latitudes 17°30′S and 56°30′S (more than 4000 km), and is divided into 15 administrative regions. The geography of the country is dominated by steep mountainous terrains, with only around 20% of the territory being flat (Figure 2(a)). The territory includes 101 main hydrologic catchments, with more than 300 rivers flowing mainly westward into the ocean (Figure 2(b)). Chile is also characterized by a wide variety of landscapes. From a geomorphological point of view, it is possible to distinguish four major geographical units along the country: Andes Mountains (East), Intermediate Depression, Coastal Mountains, and Coastal Plains (West) (Valdés-Pineda *et al.*, 2014).

The rain gauges data set was provided by the National Water Resources Directorate of Chile (DGA), and is available at http://www.dga.cl/Paginas/default.aspx. This public institution manages more than 3000 gauge stations in the country to measure different hydro-meteorologic variables. From this collection, a total of 671 operating rain gauges were used to determine their length

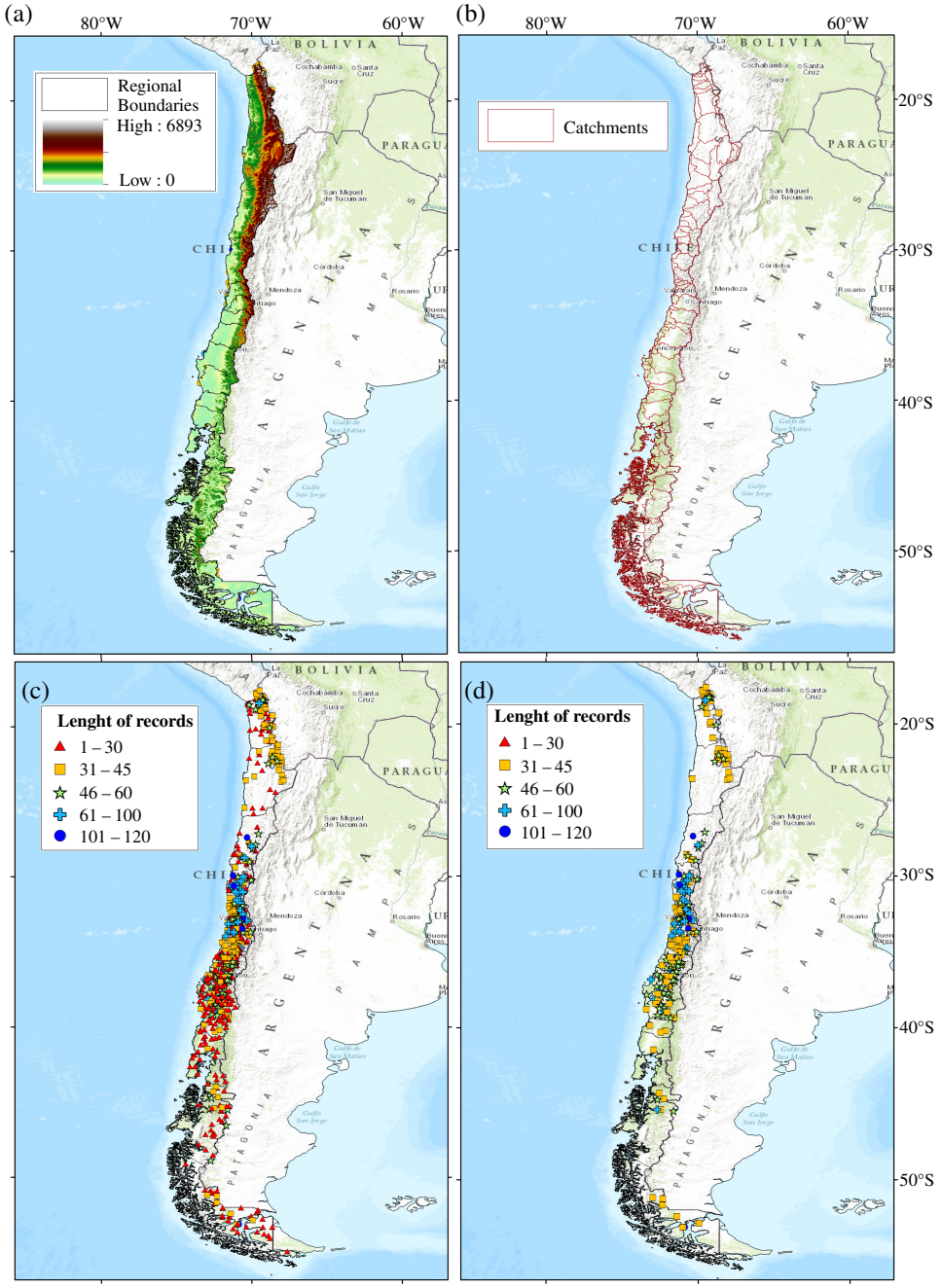

Figure 2. (a) Elevation map with administrative regions; (b) distribution of main catchments in Chile; (c) DGA's National Rain Gauges Network of Chile, (d) and the 238 rain gauges used in this study. Shaped-marker colour represents the length of records at each rain gauge between 1893 and 2012.

of records and missed data (Figure 2(c)). A systematic data quality control process was conducted for each rain gauge, taking into account only those years with at least 10 months of data. In addition, for any period of analysis, only those rain gauges with at least 90% of annual/seasonal data were selected, and only for those records that contained at least 30 years of data. The annual/seasonal time series for each defined period were sorted from north to south and then assembled in matrix form (A_{ij} = accumulation for time i at station j). Then, K-means cluster analysis was used to determine the level of correlation between the series of every pair of stations as a criterion for clustering (i.e. see Spath, 1985). These levels of correlations and different clusters of stations were finally used to fill in missing data through the K nearest-neighbour method (K_{NN}), considering the ten nearest-neighbours with weights inversely proportional to the distances expressed by $K_{\mathrm{NN}} = \frac{1}{1-\rho}$, where ρ is the correlation coefficient from the neighbouring stations (Fix and Hodges, 1989). After this, the final consolidated data set contained records spanning between 1893 and 2012 (Figure 2(d), Table 1). For instance, the shortest selected period was 1979–2012 (34 years), which represented the largest spatial coverage.

Table 1. Seasonal time-lagged correlations between $PC1_{Annual}$ and S_{CI} for the period 1979–2012.

Climatic index		AAO	SOI	PDO	MEI	ONI	TWI	N34	TNI	MJO6	MJO7	MJO8	MJO9	BEST
$SON_{(t)}$	Correlation r	−0.17	−0.50	**0.46**	**0.58**	**0.58**	−0.30	**0.56**	−0.06	**−0.52**	**−0.48**	**−0.36**	0.14	**0.56**
	t-Test	−0.99	−3.30	**2.92**	**4.07**	**3.99**	−1.77	**3.86**	−0.36	**−3.41**	**−3.12**	**−2.20**	0.80	**3.85**
$JJA_{(t)}$	Correlation r	−0.16	**−0.63**	0.19	**0.59**	**0.61**	0.00	**0.58**	−0.07	**−0.60**	**−0.37**	0.32	**0.59**	**0.66**
	t-Test	−0.93	**−4.65**	1.09	**4.19**	**4.39**	0.02	**4.06**	−0.41	**−4.19**	**−2.27**	1.93	**4.13**	**4.91**
$MAM_{(t)}$	Correlation r	−0.26	−0.21	0.04	0.08	0.10	−0.02	0.10	−0.08	−0.21	−0.16	−0.07	0.13	0.22
	t-Test	−1.55	−1.23	0.24	0.45	0.54	−0.09	0.58	−0.47	−1.23	−0.92	−0.41	0.74	1.25
$DJF_{(t)}$	Correlation r	−0.14	0.16	−0.02	−0.22	−0.18	0.31	−0.17	−0.20	−0.13	0.05	0.25	**0.38**	−0.15
	t-Test	−0.82	0.93	−0.10	−1.28	−1.01	1.83	−0.99	−1.12	−0.73	0.27	1.47	**2.34**	−0.87
$SON_{(t-1)}$	Correlation r	0.17	0.16	−0.16	−0.24	−0.26	**0.39**	−0.27	−0.28	0.19	0.36	**0.51**	**0.44**	−0.19
	t-Test	0.96	0.91	−0.93	−1.40	−1.50	**2.39**	−1.56	−1.67	1.11	2.20	**3.31**	**2.80**	−1.11
$JJA_{(t-1)}$	Correlation r	−0.04	0.35	−0.16	−0.24	−0.27	0.24	−0.29	−0.16	0.20	**0.44**	0.40	0.10	−0.28
	t-Test	−0.20	2.12	−0.91	−1.42	−1.57	1.38	−1.71	−0.90	1.14	2.78	2.50	0.57	−1.67
$MAM_{(t-1)}$	Correlation r	−0.15	0.09	0.05	−0.05	−0.11	0.00	−0.13	−0.01	0.00	0.07	0.14	0.19	−0.11
	t-Test	−0.85	0.50	0.30	−0.28	−0.62	0.00	−0.76	−0.07	0.00	0.38	0.78	1.09	−0.64
$DJF_{(t-1)}$	Correlation r	−0.21	−0.16	−0.02	0.05	−0.01	0.04	−0.01	0.07	−0.16	−0.29	**−0.36**	−0.20	0.09
	t-Test	−1.23	−0.89	−0.12	0.29	−0.03	0.22	−0.05	0.40	−0.93	−1.72	−2.20	−1.16	0.49

The t-test critical region corresponds + to $t_{(n-2;\ \alpha=0.05)} = \pm 2.037$ for $n = 34$ years with two degrees of freedom. The hypothesis is that H_0: $r = 0$, and H_1: $r \neq 0$. Bold values correspond to significant correlations at each time scale. The subscript t represents the same year.

2.2. Climate indices

The influence of climate teleconnections on precipitation variability in the subtropical and extratropical regions of Chile has been well defined in the last few decades. For instance, heavy rainfall in northern Chile occurs either during austral summer – at the mature stage of El Niño in connection with warmer SST and atypical jet streams off northern Chile – or during the previous austral winter–spring (Vargas *et al.*, 2007). Regional and large-scale circulation features during extreme rainfall conditions in central Chile (see Santiago as example in Figure 3) also share significant relationships to those observed during extreme ENSO phases (Rutllant and Fuenzalida, 1991; Aceituno and Garreaud, 1995; Garreaud and Batisti, 1999; Montecinos and Aceituno, 2003; Garreaud *et al.*, 2009). The interdecadal precipitation variability in central Chile is linked to the PDO (Montecinos and Aceituno, 2003; Garreaud *et al.*, 2009; Quintana and Aceituno, 2012), and the intra-seasonal variability is mostly modulated by the propagation of the MJO (Carrasco, 2006; Barrett *et al.*, 2012). The AAO modulates precipitation anomalies in southern Chile (largest at 40°S) and along the subtropical east coast of the continent (Garreaud *et al.*, 2009; Villalba *et al.*, 2012).

In keeping with study objectives, 13 Seasonal Climate Indices were calculated from the original monthly records of the SOI, MEI, Oceanic Nino Index (ONI), Trade Winds Index (TWI), Niño 3.4 (N3.4), Trans Nino Index (TNI), AAO, BEST, and PDO. (For a detailed description of the coupled ocean-atmosphere indices used in this research, refer to Section I of the Appendix S1.) The daily values of MJO were first aggregated at a monthly scale and then at a seasonal scale. MJO is associated with ten particular phases that represent different conditions as the MJO oscillation progresses eastward from the Indian Ocean through the Pacific Ocean (Madden and Julian, 1971, 1972; Zhang, 2005; Barrett *et al.*, 2012). Accordingly, we only selected the phases 6, 7, 8, and 9 because they represent enhanced convection conditions over the South American continent. The seasonal averaged indices were calculated as:

$$S_{\mathrm{CI}_k} = \frac{\sum_{i=1}^{n} \mathrm{CI}_{ij}}{n} \tag{1}$$

where, S_{CI_k} is the Seasonal Climate Index for a single year k. CI_{ij} is the Climate Index of the month i (where $i = 1 \ldots 3$), within the season j (where $j = 1 \ldots 4$, and $j_1 = \mathrm{DJF}$; $j_2 = \mathrm{MAM}$; $j_3 = \mathrm{JJA}$; and $j_4 = \mathrm{SON}$). n is the number of months within each season ($n = 3$).

2.3. Spatial relations and seasonal ratio index

As a way of accounting for any spatial effect in the accumulation patterns, such as those previously described in the Section 1, the relationship between annual/seasonal precipitation and the geographic position (latitude, longitude, and elevation) of each rain gauge was initially mapped and analysed. The spatio-temporal distribution of seasonal precipitation accumulation (mm) compare to annual precipitation accumulation (mm) was additionally computed for each year and for each station using the seasonal ratio index ($\mathrm{SR_I}$) as: $\mathrm{SR_I} = \left[\frac{\mathrm{Sac}_i}{\mathrm{Aac}_i}\right]$, where Sac_i is the seasonal accumulation for the year i (mm), and Aac_i is the annual accumulation for the year i. The $\mathrm{SR_I}$ for any year can be represented as decimal numbers (or percentage) ranging between 0 and 1 (0–100%). The length of the S_{CI} time series varied: the longest was from 1854 to present for the SOI (which was mainly used to detect patterns of longest rain gauges series); the shortest were for MJO and AAO oscillations, from 1978 and 1979 onward, respectively.

2.4. Annual and seasonal SPI calculation

At each rain gauge, the annual and seasonal series of precipitation accumulation were standardized by

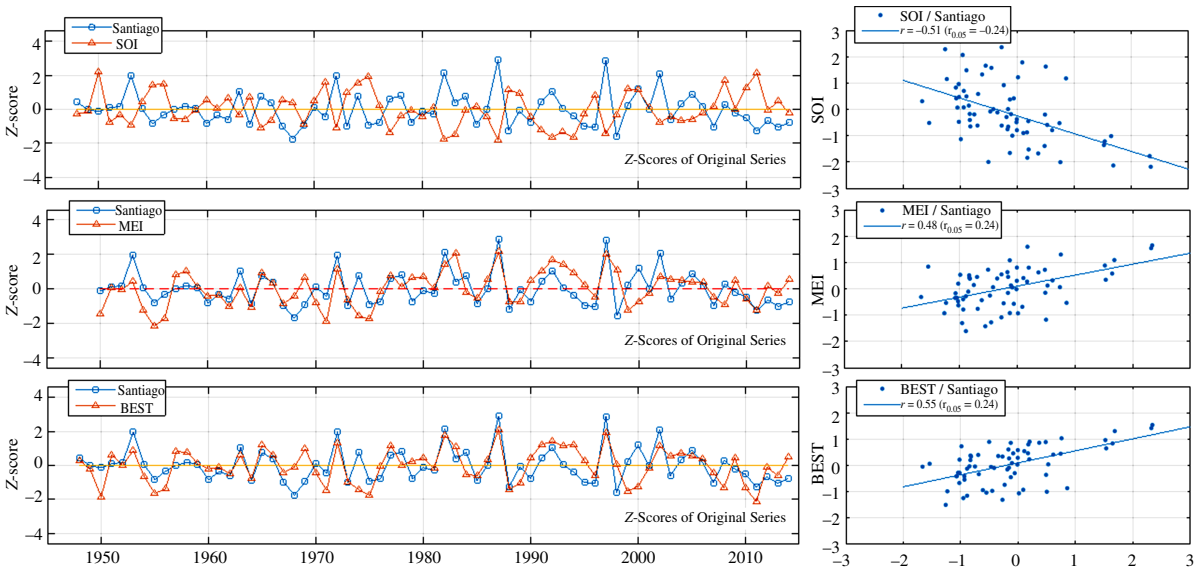

Figure 3. Standardized time series (left panels) and scatter plots (right panels) of correlations between ENSO indices SOI, MEI, BEST, and precipitation in Santiago de Chile between 1948 and 2012.

using the 12-month Standardized Precipitation Index (SPI), which was calculated following the procedure of McKee *et al.* (1993). Conceptually, the SPI represents a *z*-score, which is the number of standard deviations above or below the zero-mean (see Section III of the Appendix S1). This index is the current technique used by the National Oceanic and Atmospheric Administration (NOAA) to monitor droughts in United States (http://www.cpc.ncep.noaa.gov/products/Drought/Monitoring/spi.shtml). Over the last decade, SPI has increasingly been used for assessment of drought intensity in many countries (Vicente-Serrano *et al.*, 2004; Wilhite *et al.*, 2005; Wu *et al.*, 2006; Karavitis *et al.*, 2011; Mwangi *et al.*, 2014; Bonaccorso *et al.*, 2015). When compared to other drought indices, the SPI has demonstrated favourable performance (Guttman, 1998; Keyantash and Dracup, 2002; Zarch *et al.*, 2015). Vicente-Serrano *et al.* (2010) made a modification to create the Standardized Precipitation Evapotranspiration Index (SPEI), which is based on precipitation and temperature data. Bazrafshan *et al.* (2014) and Beguería *et al.* (2014) established the Multivariate Standardized Precipitation Index (MSPI), with which it is possible to aggregate a variety of SPI time series into new time series. In Chile, Verbist *et al.* (2010) implemented the SPI Index approach in the Coquimbo Region (29°54′S latitude 70°15′W longitude) of Chile by calculating the index at seasonal scales, with the objective of designing a drought early warning system for risk management support. Currently, SPI is also used by the Chilean National Weather Service (www.meteochile.gob.cl/prediccion_estacional.php) and by the Drought Monitor System of the Ministry of Agriculture of Chile (http://www.climatedatalibrary.cl/UNEA/maproom/).

The SPI classification (see Section IV of the Appendix S1) proposed by the National Drought Mitigation Center of the University of Nebraska-Lincoln (http://drought.unl.edu/) consists of seven classes ranging from negative values for dry conditions ($-2.0 \leq \mathrm{SPI} \leq -1.0$), to positive values for wet conditions ($1.0 \leq \mathrm{SPI} \leq 2.0$). This classification was used in this study to evaluate the probability of observing very and extremely wet conditions $P(\mathrm{SPI} \geq 1.5)$, or observing very and extremely dry conditions $P(\mathrm{SPI} \leq -1.5)$, using data of El Niño and La Niña events recorded between 1979 and 2012 (238 rain gauges).

2.5. EOF analysis for annual and seasonal precipitation

Several empirical orthogonal functions (EOF) analyses or also called principal component analysis (PCA) have been conducted in South America (Chile) during the last few decades. Using infrared data from geostationary satellites ($0.5° \times 0.5°$ of spatial resolution), Garreaud and Wallace (1997) applied EOF analyses to seasonal mean 3-h anomalies of the cold cloud coverage (defined for each grid as the fraction of temporal samples that exhibited cloud-top temperatures colder than 235 K). Searching for dominant modes of the variability of convective cloudiness on synoptic timescales, Garreaud and Wallace (1998) applied EOF analysis to the daily anomalies of the Convective Index over South America. Montecinos and Aceituno (2003) analysed the seasonality of the ENSO rainfall in central Chile and associated circulation anomalies through a seasonal rainfall index defined as the first principal component (PC1) of standard deviation–normalized rainfall series. Aravena and Luckman (2009) used PCA and singular spectrum analysis (SSA) to analyse annual spatial and temporal patterns from a network of 23 rain gauges located in southern South America (40°S southward). Montecinos *et al.* (2011) used the first PCA of standardized rainfall anomalies during 24 non-ENSO winters in the period 1958–2000, calculated from records of 63 ground stations (30°–42°S), in order to analyse the non-ENSO interannual

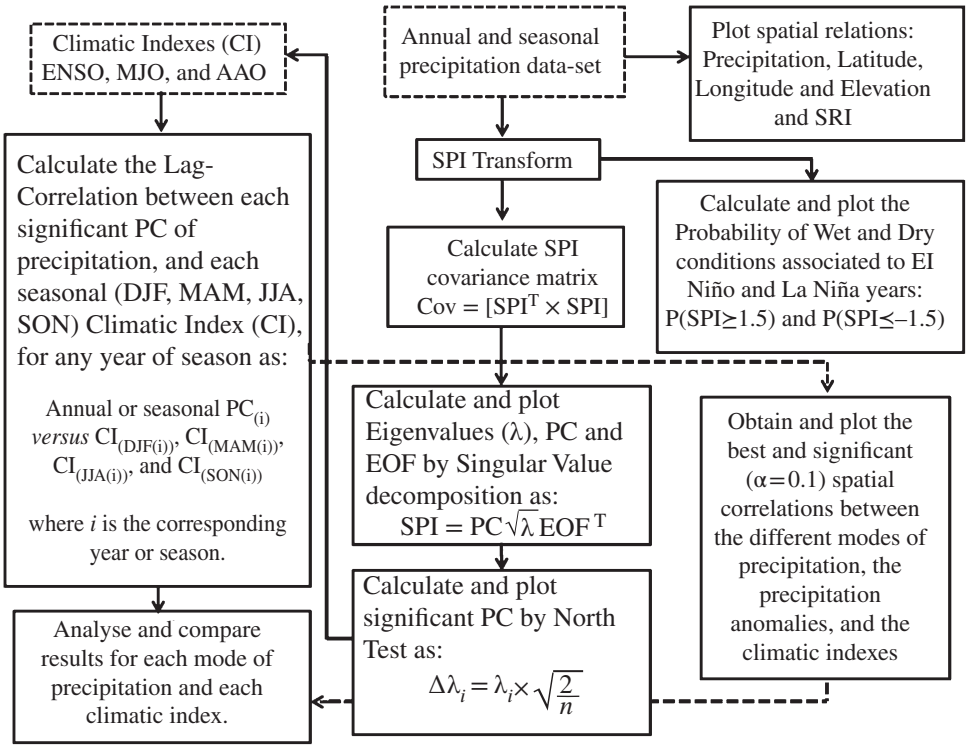

Figure 4. Methodological steps used in this study to describe annual and seasonal precipitation patterns.

rainfall variability in central Chile during austral winter. Zamboni *et al.* (2012) used EOF analysis to determine seasonal variations and links between the interannual precipitation variability of South America and the South Pacific. Most of these studies were focused on analysing modes of interannual variability; therefore, a seasonal resolution would allow for the establishment of currently unidentified spatio-temporal patterns that could explain the seasonal precipitation variability in the country. Accordingly, in this study, we calculated the leading modes of annual and seasonal precipitation, and their degree of correlation to different climatic oscillations and other gridded data sets. (For a detailed description of EOF analyses carried out in this study, refer to Section V of the Appendix S1.) For instance, to study how the main modes of annual and seasonal precipitation variability (rain gauges) are associated with zonal winds, SLP, and SST, we projected each gridded field onto the PC1 (of annual and seasonal precipitation) in order to obtain the global signature (but mainly focused on the Pacific Basin) associated with each leading mode.

2.6. Significant leading modes of precipitation variability

In order to decide which EOF/PCA to retain (or discard), North *et al.* (1982) proposed a test to define typical errors between two neighbouring eigenvalues λ (or eigenvectors). Accordingly, the North test was used to evaluate the statistical significance of each leading mode of annual/seasonal precipitation at the 95% level, assuming each year is independent. The statistical significance was calculated with to the following equation:

$$\Delta\lambda_i = \lambda_i\sqrt{\frac{2}{n}} \tag{2}$$

where, $\Delta\lambda_i$ is the confidence interval at the 95% level of significance for the explained variance. λ_i is the ith eigenvalue. n is the sample size.

Then the first ten eigenvalues with error bars (scaled as percentage of explained variance) were plotted for annual/seasonal precipitation patterns in order to determine their significant modes of annual and seasonal precipitation patterns.

2.7. Climate oscillations and their relationship to leading modes of precipitation

Each significant leading mode of annual and seasonal precipitation (PC) was correlated to precipitation anomalies at each rain gauge, and also using gridded data from NOAA (see Section 3.7). The statistical significances were evaluated using the t-test ($\alpha = 0.05$). This analysis allowed for the determination of the different point- and gridded-based spatial patterns that dominate annual and seasonal precipitation variability in Chile. In addition, seeking to determine which seasonally aggregated climate indices were significantly related to these spatial patterns, a seasonal time-lagged correlation coefficient was also calculated for the relationship between each significant PC $\left(S_{\mathrm{PC}_i} = \mathrm{PC}_1,\ \mathrm{PC}_2, \mathrm{PC}_3,\ \ldots\ ,\ \mathrm{PC}_n\right)$ and each seasonally aggregated index $\left(S_{\mathrm{CI}_i} = S_{\mathrm{CI}_1}, S_{\mathrm{CI}_2}, S_{\mathrm{CI}_3},\ \ldots\ , S_{\mathrm{CI}_{n-1}}\right)$, considering up to 1-year back of correlations (four seasons). The significances of these correlations were also

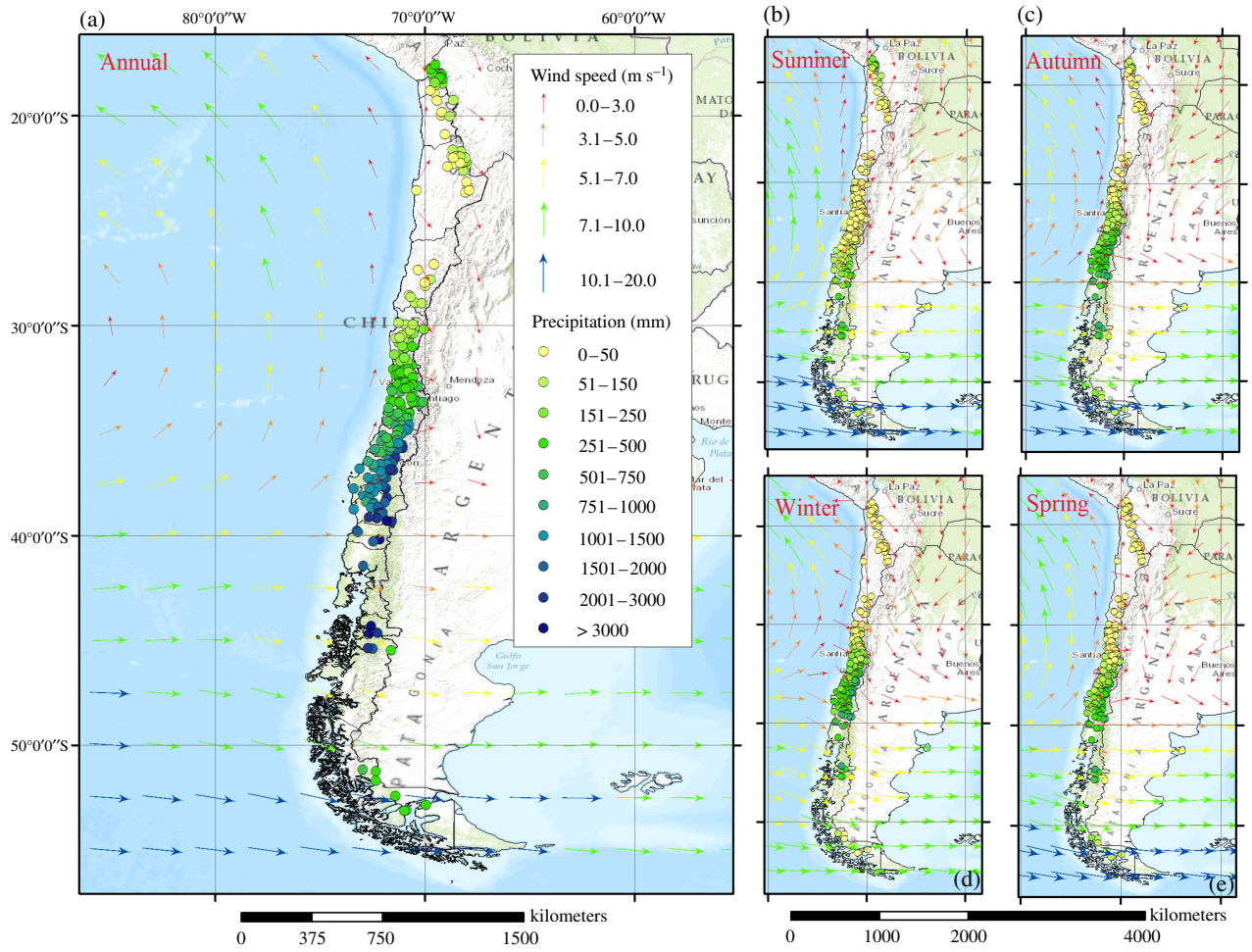

Figure 5. Spatial distribution of averaged annual and seasonal precipitation accumulations (mm) for 238 ground stations (1979–2012) distributed through the country and 925-hPa zonal and meridional wind (m s^{-1}) components (U925; V925). The legend on the annual map is also scaled for seasonal patterns.

calculated using a *t*-test ($\alpha = 0.05$). The point of applying the time-lagged correlation analysis was to identify which seasonally aggregated index was significantly influencing annual/seasonal precipitation variability in Chile. The methodological steps used in this study are summarized in Figure 4.

3. Results

3.1. Spatial patterns of precipitation accumulation

The spatial distribution of average annual and austral summer precipitation accumulation in Chile shows a marked latitudinal decrease in Northern regions with an evident North-to-South gradient (Figure 5(a) and (b)). This latitudinal gradient goes from nearly 400 mm year^{-1} over the Altiplano (~18°S) to about 20 mm year^{-1} in the Atacama Desert Region (~27°S). This is due to the fact that the most-northern regions receive a larger contribution of precipitation during the austral summer, caused by strong convection and daily moisture movement from the Amazonia during SAMS (see also Fuenzalida and Ruttlant, 1987; Horel *et al.*, 1989; Garreaud and Wallace, 1997; Vuille *et al.*, 1998; Garreaud, 1999; Vuille, 1999; Garreaud, 2000; Garreaud and Aceituno, 2001; Garreaud *et al.*, 2003; Houston and Hartley, 2003; Houston, 2006; Minvielle and Garreaud, 2011). A second latitudinal gradient is observed from 27°S southward, along Central Chile (Falvey and Garreaud, 2007), as a result of the North–south movement of westerlies (see Rahn and Garreaud, 2014). This pattern reaches its annual and seasonal maxima between 40° and 45°S (see Figure 6), where precipitation accumulation can increase up to more than 150 times. For instance, more than 3000 mm year^{-1} (on average) can be registered in Northern Patagonia; this total is typically distributed as ~500 mm in summer; ~800 mm in autumn; ~1000 mm in winter; and ~700 mm in spring. However, some rain gauges can even register more than 4000 mm year^{-1} along the western Andes (as reported by Carrasco *et al.*, 2002; Villarroel, 2013; Viale and Garreaud, 2015; Valdés-Pineda *et al.*, 2015). This large amount of precipitation is due to the fact that south of 40°S the low-level westerly flow prevails year-round and most of the rainfall is produced by deep stratiform clouds that develop along warm and cold fronts (Garreaud *et al.*, 2009). A third latitudinal gradient reveals a decrease

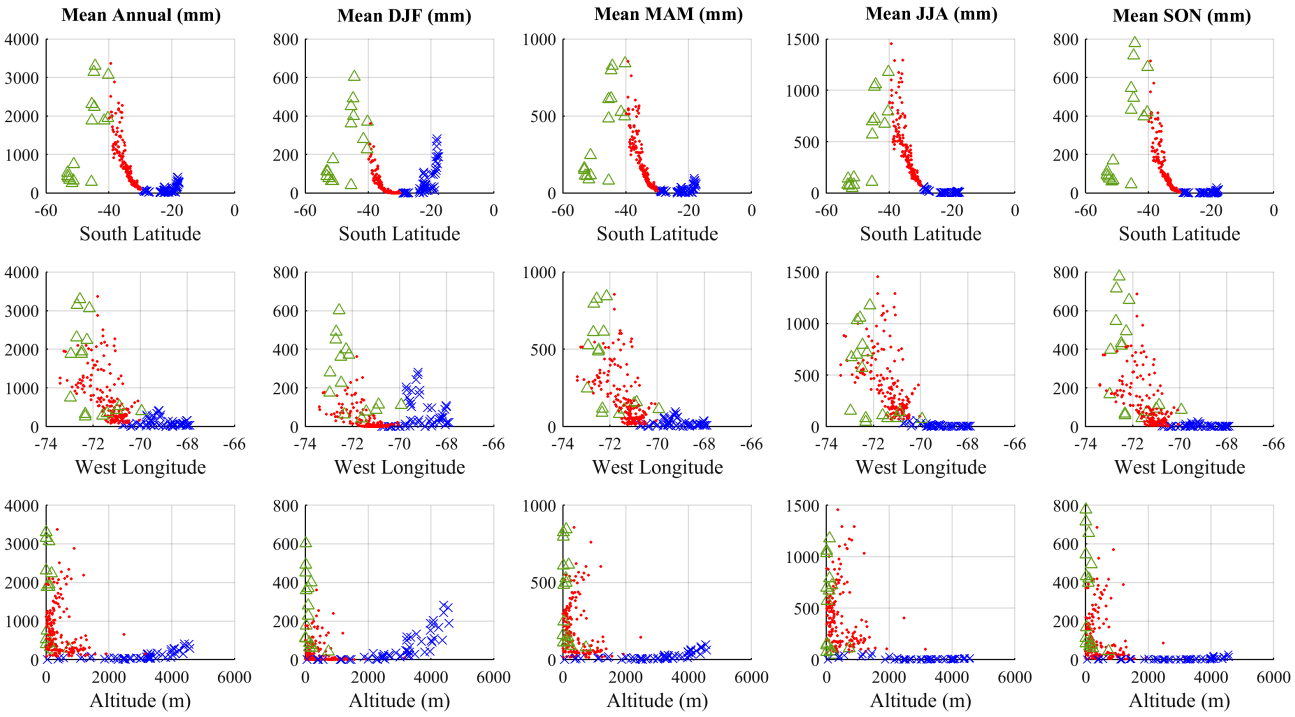

Figure 6. Scatter plots between mean annual and seasonal precipitation (mm) for 238 ground stations (1979–2012) distributed in Chile, and latitude, longitude, and altitude. Marker colour represents northern Chile (blue-x), central Chile (red-circle), and southern Chile (green-triangle).

southward, reaching minimum annual accumulations of ∼250 mm in those rain gauges located between 51° and 53°S (Figure 5(a)). Because the low-level westerlies expand equatorward during austral winter, but weaken predominantly in Patagonia south of 50°S (see Figure 5(b) and (d)), the larger contribution to annual precipitation is mostly observed during austral autumn (up to 1.8 times larger) rather than austral winter (Figure 5(c) and (d)). This latter season even registers similar amounts to those recorded during the austral summer and spring; i.e. seasonally averaged precipitation accumulation ranging between ∼50 and ∼150 mm (Figure 5(b) and (e)). These results also are consistent with the analysis of Carrasco *et al.* (2008) on the basis of average monthly distribution of precipitation in Chile.

The described North-to-South (down-up-down) latitudinal gradient of annual and seasonal precipitation accumulation can be clearly shown through scatter plots developed for the whole country (upper plots in Figure 6). For instance, a linear decay is observed in Northern Chile that is stronger during austral summer ($r = 0.74$) but weakens during austral winter ($r = 0.55$), and remains more or less constant during autumn and spring. Then an exponential growth is evident along the Central part of the country; it is stronger at annual scale ($r = 0.95$) but also noticeable at seasonal scale ($r \geq 0.90$). In the Southern regions, a linear decrease is more evident during austral winter ($r = 0.84$), but also significant during the other three seasons ($r \geq 0.80$). On the other hand, larger variability was noticed for the relationships between precipitation accumulation and West longitude or altitude (middle and lower plots of Figure 6). This variability can be attributed to the Andean orography, which varies intensely along the country and generates different local conditions of orographic enhancement (OE) that cannot be clearly detected when the data are arranged at a national scale. Accordingly, the Andean orographic influence on precipitation accumulation is revised in detail in the following section.

3.2. Orographic effects on precipitation accumulation

The average height of the Chilean Andes surpasses 4000 m.a.s.l. in the subtropical latitudes (18°–35°S), and the average width of the range is less than 200 km (Figure 7(a) and (b)). The average height rapidly decreases southward, dropping to less than 1500 m.a.s.l. in the extratropical latitudes (40°–55°S); in that area the width can increase up to about 400 km, forming an elevated plateau (Garreaud *et al.*, 2009; Viale and Garreaud, 2015). In Northern Chile, most of the annual precipitation accumulation originates from mid- and upper-level easterly winds that transport moist air from Amazonia to feed convective storms over the eastern Andes during the austral summer (Minvielle and Garreaud, 2011). As a consequence, drier conditions are observed on the western side of the Andes, where precipitation accumulation can decrease more than 20 times due to rain shadow. This altitudinal gradient is highly linear between 2000 and 4500 m.a.s.l. (17–21°S) at annual and seasonal scales, being stronger during austral summer and autumn but also significant during austral winter and spring (Figure 7(a)).

In Central Chile, westerlies carrying frontal systems to the continent are blocked by the Andes, generating an OE which is evident at annual and seasonal scales

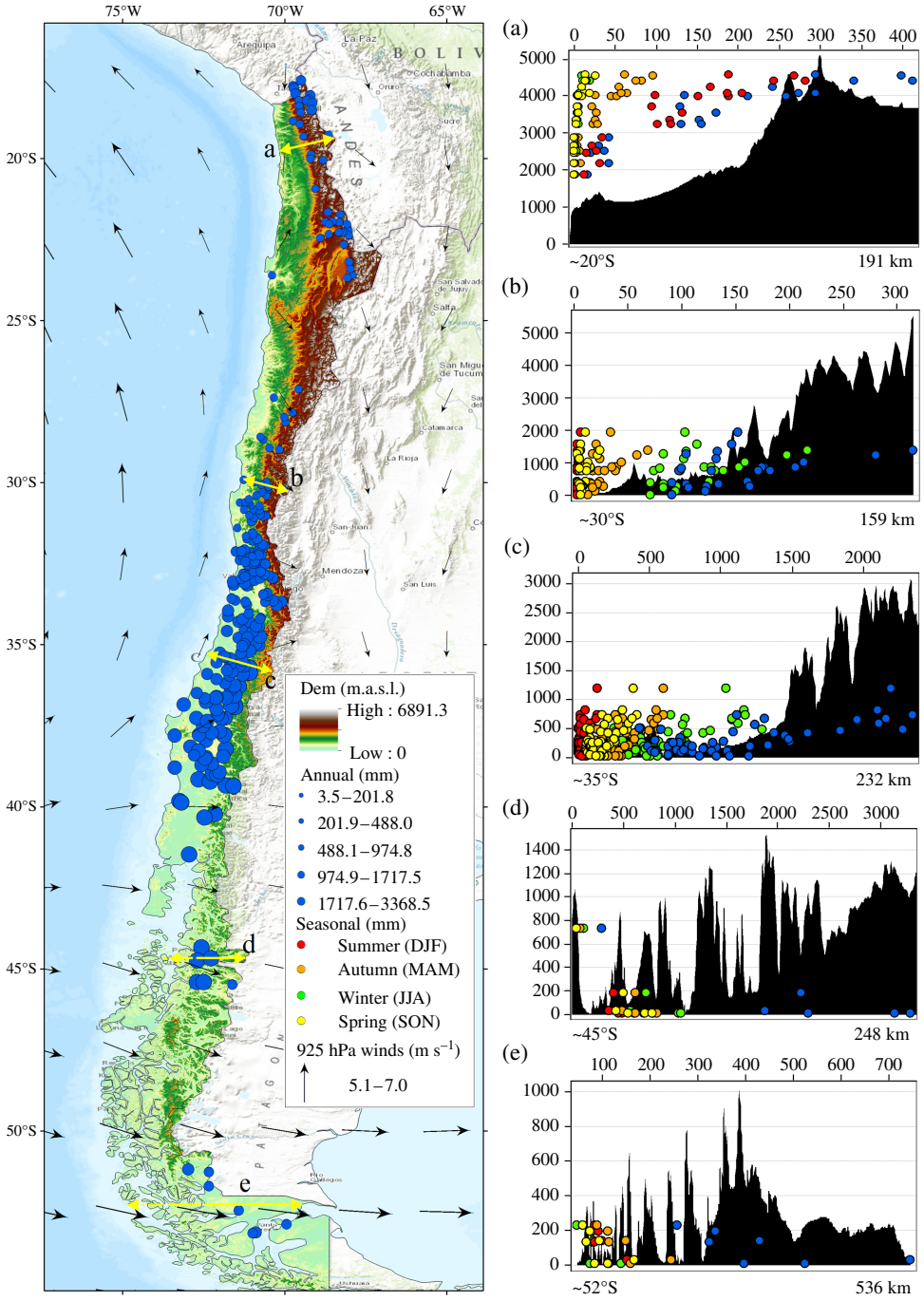

Figure 7. Topographic transects (a–e), for different subtropical and extratropical latitudes in Chile (left-map). These transects are represented on the right plots as elevation profiles (black). The left axis represents the elevation in metres above sea level (m.a.s.l.), while the upper axis is annual or seasonal accumulation in millimetres (mm), represented as scatter plots for those rain gauges distributed in the following bands: (a) 17°–21°S; (b) 29°–31°S; (c) 34°–37°S; (d) 44°–45°S; and (e) 51°–53°S. Black arrows represent mean annual 925-hPa zonal and meridional wind (m s^{-1}) components (U925; V925).

(see Falvey and Garreaud, 2007; Viale and Garreaud, 2015). The enhancement rates (ER) associated with annual accumulation can reach to more than four times between 0 and 2000 m.a.s.l. The seasonal ER ranges from three during austral winter to more than five during autumn and spring (Figure 7(b) and (c)). During austral summer, precipitation accumulation can surprisingly increase more than 15 times in the cross-mountain direction at about 30°S (Figure 7(b)). This ER is much more significant south of 35°S (ER > 20) since a latitudinal increase is observed in summer precipitation (Figure 7(c)).

In Southern Chile, the monthly precipitation variability is strongly negatively (positively) correlated with 850-hPa zonal wind speed in eastern (western) Patagonia. This means that a year (or season) with stronger than average low or mid-level westerly flow features increased precipitation to the west of the Andes and decreased precipitation over the lowlands to the east due

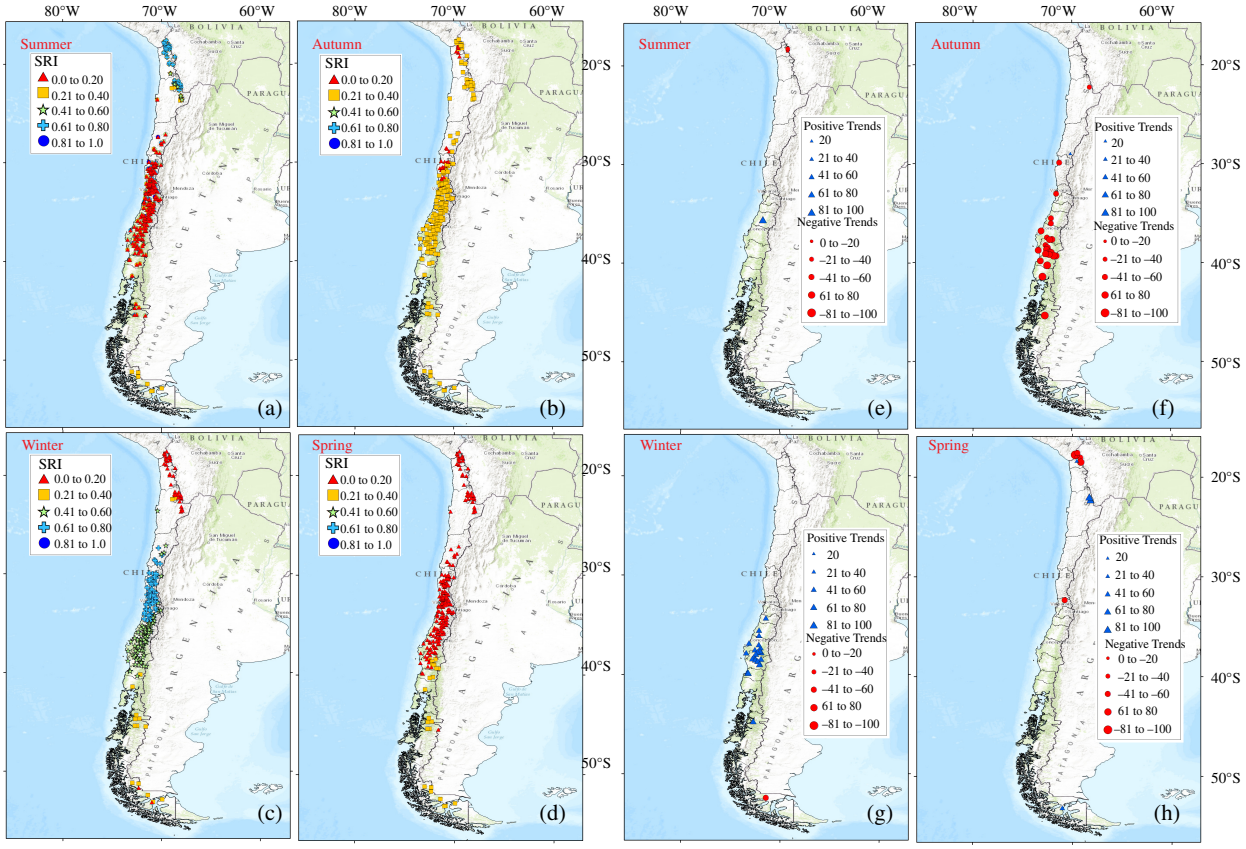

Figure 8. (a–d) Seasonal Ratio Index for 238 rain gauges (1979–2012) where shaped-marker colour represents the average SR_I; (e–h) significant Mann–Kendall trends of SR_I in Chile, where marker-size represents changes in units of percentage.

to rain shadow (Garreaud *et al.*, 2013). This pattern is clearly detected from the group of stations distributed around 45°S (0–100 m.a.s.l.), and those located about 52°S (0–250 m.a.s.l.) where a strong (linear) altitudinal decrease is observed because a larger proportion of precipitation is registered over the Pacific Ocean at annual and seasonal scales (Figure 7(d) and (e)).

3.3. Seasonal ratio index

The averaged SR_I calculated for those rain gauges distributed along the band 18°–25° reveals that between 60 and 80% of the annual accumulation occurs during the austral summer. Along the regions located between 25° and 45°S, summer precipitation consistently contributes less than 20%; however, this percentage is slightly exceeded in stations located in the band 50°–55°S (Figure 8(a)). The autumn contribution is concentrated between 20 and 40% for most of the country (Figure 8(b)). During the austral winter, precipitation accumulation is commonly less than 20% of annual precipitation for most of the stations located in northern regions (≤25°S). An increase in winter contribution is then observed between 25° and 30°S, reaching a peak of about 80% at this latter latitude. Then the winter contribution gradually decreases to less than 20% in some cases in southern rain gauges along the band 50°–55°S (Figure 8(c)). Lower spring contribution ($SR_I \leq 20\%$) is observed in those rain gauges located north of 40°S, and higher spring contribution (∼20%) was observed in stations located south of 40°S (Figure 8(d)). Temporal trends of SR_I calculated for all rain gauges (Mann–Kendall test) revealed significant positive (negative) changes during austral summer (spring) between 1979 and 2012 for some rain gauges in Northern Chile (Figure 8(e) and (h)). These changes are more noticeable in Central and Southern Chile for those rain gauges located around 40°S, which showed mostly significant negative (positive) trends during austral autumn (winter) (Figure 8(f) and (g)). Seasonal changes have recently been reported for United States by Allen and Sheridan (2015), who analysed temperature data concluding that late starts of autumn and winter have been observed while earlier onsets of spring and summer have taken place between 1948 and 2012.

3.4. SPI and ENSO conditions

Results for northern Chile have to be taken with caution, because the large number of years with zero precipitation in the records causes some wet years to easily exceed very and extremely wet conditions ($SPI \geq 1.5$) as defined by the SPI classification (Figure 9(a)–(c)). In central and southern Chile, SPI can adequately represent the drought conditions. For instance, the 'Great Drought' occurring in central Chile between 1968 and 1969 is clearly represented by records of more than 100 years, showing negative values of SPI larger than extremely dry conditions (Figure 9(d)–(f)). The recent 2007–2008 drought

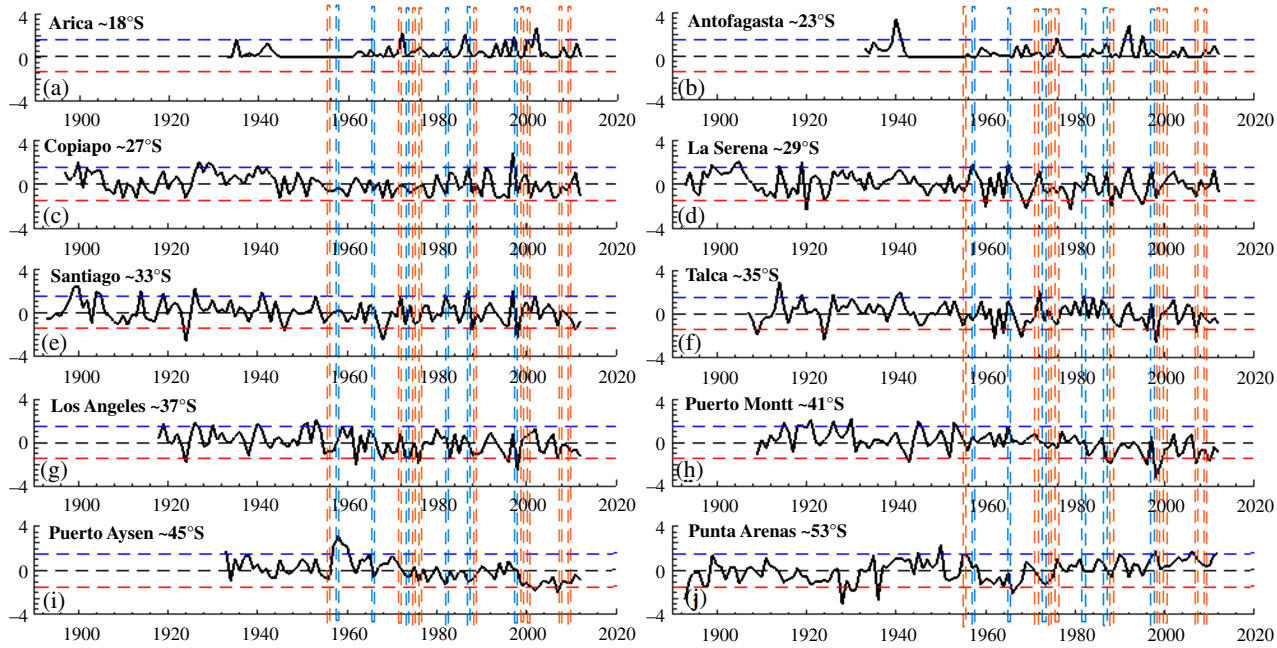

Figure 9. Annual Standardized Precipitation Index (SPI) for long-record rain gauges in Chile. The dashed blue line represents extremely and very extremely wet conditions (SPI > 1.5), and the dashed-red line represents extremely and very extremely dry conditions (SPI < −1.5). Vertical bars represent strong and very strong El Niño (blue) and La Niña (red) conditions. [According with the classification proposed by NOAA for the Oceanic Niño Index (ONI), strong El Niño years are 1957/1958; 1965/1966; 1972/1973; 1987/1988. Very strong El Niño years are 1982/1983; 1997/1998. Strong La Niña years are 1955/1956; 1970/1971; 1998/1999; 2007/2008. Very strong La Niña years are 1973/1974; 1975/1976; 1988/1989; 1999/2000; 2010/2011.]

event that affected most of the country is also evident in the records of southern rain gauges, where extremely dry conditions are clearly identified (Figure 9(g)–(j)).

Recent trends and ENSO influence on droughts in Chile between 29° and 32°S demonstrate that extreme dry events (calculated by SPEI) show negative temporal trends particularly during the austral spring and summer, which are strongly associated with a trend towards increasing drought frequency (Meza, 2013). Regional Frequency Analysis coupled with L-moments has additionally showed that droughts with 40% of the normal precipitation are associated with return periods of 4 years at around 29°S to 22 years at about 35°S (Núñez *et al.*, 2011). In accordance with previous research, this temporal pattern of above average precipitation (droughts) in central Chile should be closely related to El Niño (La Niña) conditions (see Figure 9), which are linked to weakening (strengthening) of the subtropical anticyclone allowing for the shift (blocking) of frontal storms to more northern locations. When assessing the probability of observing extreme hydrologic conditions (calculated by SPI) during strong and very strong ENSO phases, our results indicate that there is a greater probability (10–30%) of observing very wet and extremely wet conditions in Central Chile during El Niño years (Figure 10(a)). This pattern can also be observed in those rain gauges located at around 25°S due to the northward displacement of westerlies during El Niño conditions, i.e. the Antofagasta region as reported by Vargas *et al.* (2000, 2007). On the other hand, the lowest probability of observing very dry and severely dry conditions (SPI ≤ −1.5) during El Niño years is concentrated in central Chile ($P \leq 5.0\%$), with greater probabilities concentrated in southern Chile (Figure 10(b)). During La Niña years, the probability of observing very wet and extremely wet conditions is greater at around 20°S and also in the rain gauges located south of 45°S (Figure 10(c)). Intense dryness is mainly observed in central Chile during La Niña years, where the probability of very and severely dry conditions (SPI < −1.5) is greater than that observed for the rest of the country ($P \geq 20\%$) (Figure 10(d)). Although these results are consistent with previous studies, it is worth mentioning that there is a potential impact associated with the limitations of Standardized Drought Indices (SDI), which are derived by the influence of multi-decadal climate variability (Núñez *et al.*, 2014). Therefore, the relationship between a future national drought policy and whichever indices are used to make it effective will have to account for this variability.

3.5. Leading modes of annual and seasonal precipitation

Strong leading modes of annual and seasonal precipitation variability were detected at all temporal scales (1979–2012). For instance, the first principal component of annual precipitation ($PC1_{Annual}$) for the whole country is significant, explaining 55% of the total annual variance. According to the approach proposed by North *et al.* (1982), the second and third leading modes of annual precipitation are not well separated from the subsequent modes; therefore, they are not significant at the 95% confidence level (Figure 11). Similar results were found by Pezoa (2003), who used PCA to study the spatial patterns of precipitation from 57 Chilean stations between 33° and

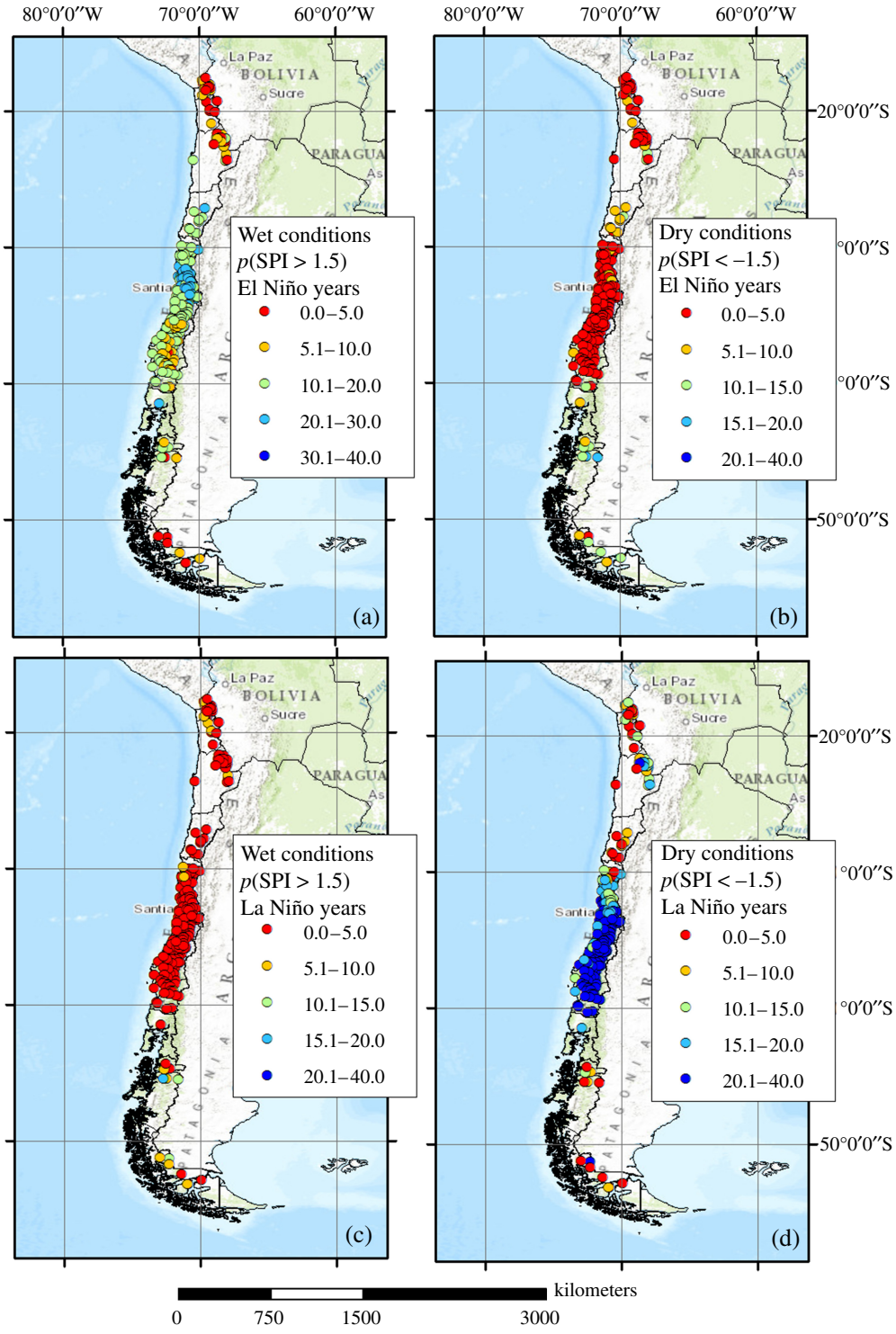

Figure 10. (a) and (c) Probability (%) of having very to extremely wet conditions $P(\mathrm{SPI} > 1.5)$; (b) and d) show the probability of having very to extremely dry conditions $P(\mathrm{SPI} < -1.5)$, associated with El Niño (a and b) and La Niña (c and d) conditions (1979–2012).

53°S (1962–2001). The first principal component (PC1) of mean annual precipitation explained 61% of the total variance and was associated with stations north of 40°S. A second PC (12%) was associated with stations around 45°S, and a third PC (5%) was associated with the Punta Arenas station (~53°S). Results of PCA for southern South America showed very strong spatial patterns for the annual rainfall records (1961–2000), depicting six significant PCs that contained more than 78% of the total variance, and a PC1 explaining 21% of the total variance (Aravena and Luckman, 2009).

The leading modes of summer precipitation showed significant components with explained variances of 46.2, 20.1, and, 8.7%, respectively (Figure 12(a)). Similar results were found for autumn and winter precipitation patterns (Figure 12(b) and (c)), demonstrating at least

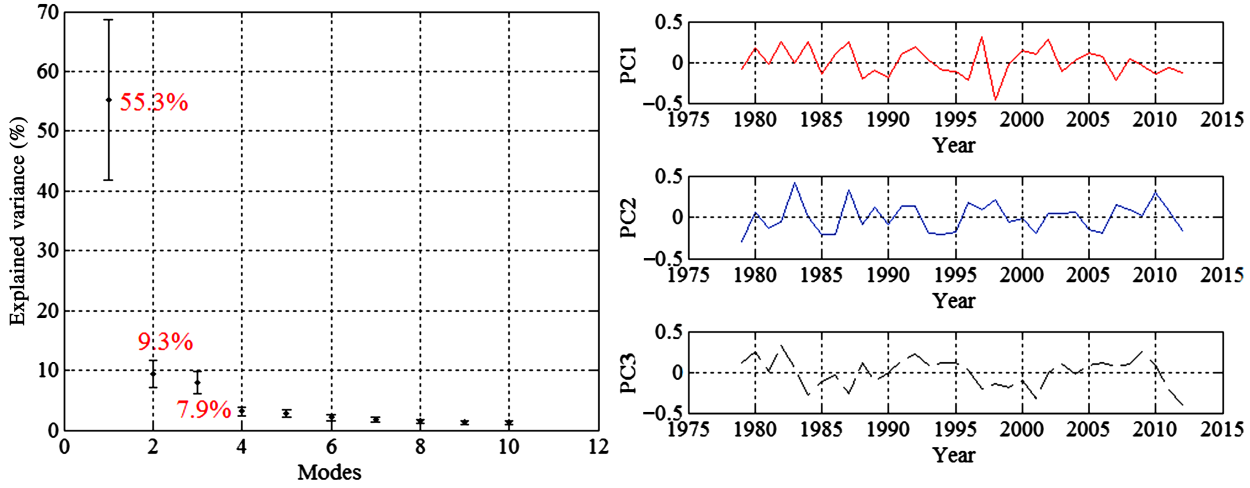

Figure 11. Eigenvalue spectrum calculated through North Test (left panel), and time series (right panel) of the first three leading modes (principal components PC1, PC2, and PC3) of annual precipitation for 238 raingauges (1979–2012).

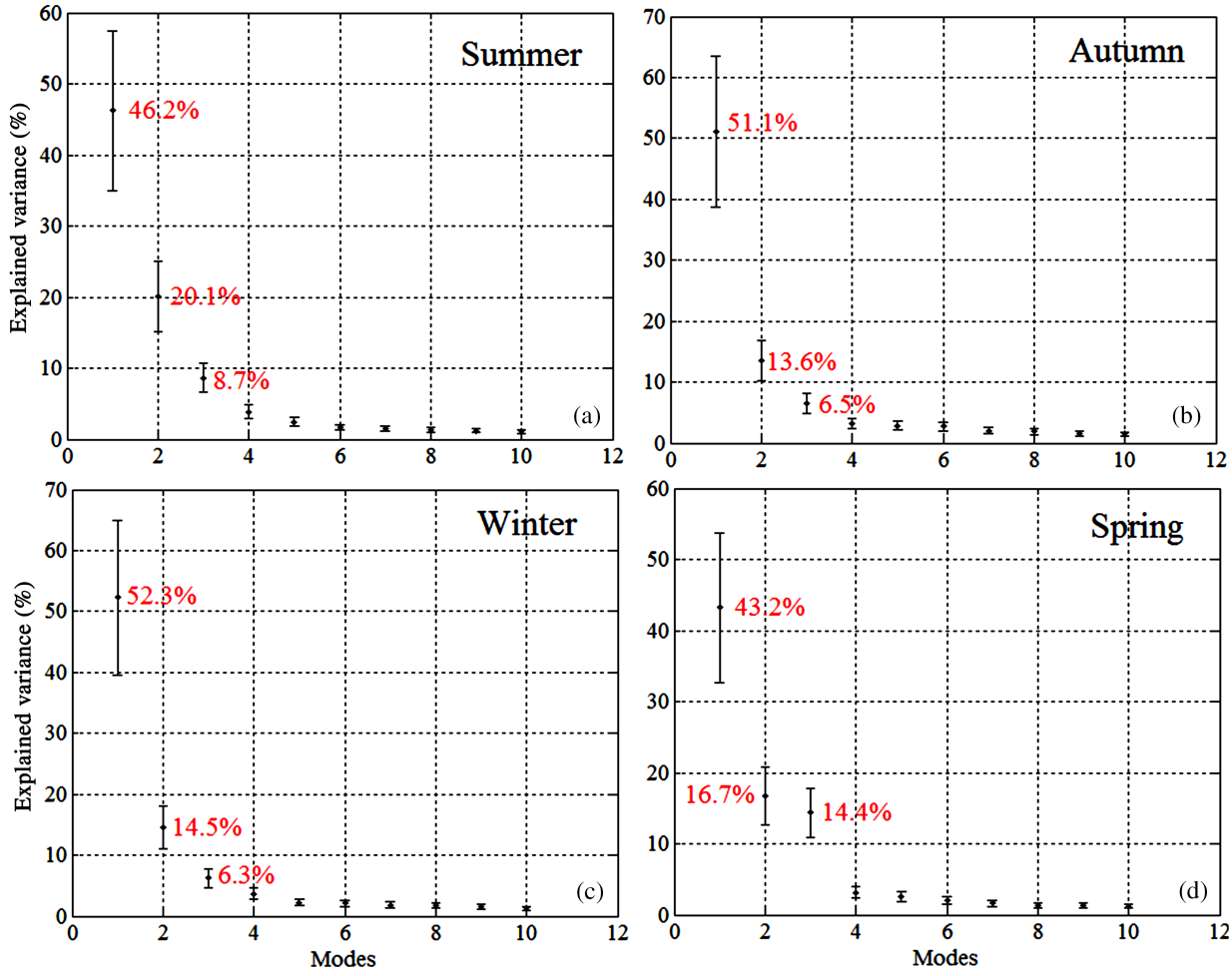

Figure 12. Eigenvalue spectrum of the covariance matrix showing the ten eigenvalues (%), i.e. explained variance of the first ten EOF/PC (modes) calculated for summer (DJF), autumn (MAM), winter (JJA), and spring (SON) precipitation accumulation (238 stations for the 1979–2012 period).

three significant modes in each season. During the austral spring, precipitation patterns were similar to those in the annual analysis since only the first leading mode of precipitation ($PC1_{Spring}$) was found to be significant. This mode also represented the smallest portion of explained variance (Figure 12(d)). Montecinos and Aceituno (2003) reported larger explained variances by calculating the PC1 of monthly standardized records of rainfall (1958–1999). The authors found explained variances of 82% (winter), 84% (late spring), and 78% (summer), for a total of 49

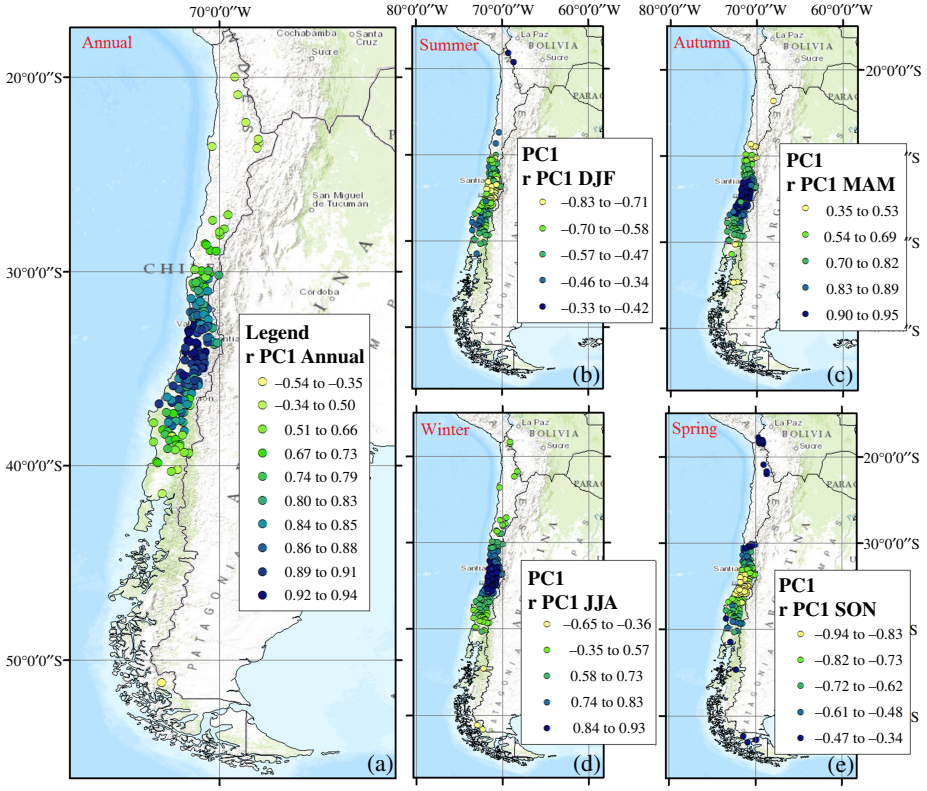

Figure 13. Significant correlation maps between the annual and seasonal precipitation anomalies and PC1. The significant correlations were calculated through t-test for $\alpha = 0.05$ (critical T-value = 2.037 for $n = 34$ years).

rain gauges distributed in three different clusters in central Chile. However, during non-ENSO winter seasons, the explained variance increases, because the PC1 of standardized rainfall anomalies during those conditions can explain up to 91% of the total precipitation variability (Montecinos *et al.*, 2011).

3.6. Anomalies and leading modes of precipitation

Correlation maps between annual (seasonal) anomalies at each rain gauge and significant leading modes of precipitation revealed varied results. For instance, the first leading mode of annual precipitation ($PC1_{Annual}$) shows positive and significant correlations between 20° and 40°S; however, a strong significant $PC1_{Annual}$ pattern is mainly concentrated in Central Chile (see also Pezoa, 2003), where the largest significant (positive) correlations can be observed between annual anomalies of precipitation and $PC1_{Annual}$. Only one rain gauge located in Southern Chile (south of 50°S) showed a significant relationship for $PC1_{Annual}$, which is negatively correlated to annual precipitation anomalies (Figure 13(a)). These most southern regions of Chile have been described by Aravena and Luckman (2009) who found four regional patterns of annual precipitation (1950–2000): Northwestern Patagonia (41°–44°S), Central Patagonia (45°–47°S), Patagonia plain-Atlantic (43°–50°S), and Southern Patagonia (51°–53°S).

At a seasonal scale, the leading mode of summer precipitation ($PC1_{Summer}$) revealed mostly negative and significant correlations in Central Chile (Figure 13(b)). On the contrary, the first leading mode of autumn precipitation ($PC1_{Autumn}$) showed positive and significant links in central Chile, with the strongest activity ($r \geq 0.85$) around 35°S (Figure 13(c)). The significant mode of winter precipitation ($PC1_{Winter}$) showed similar patterns to those observed at an annual scale: positive and significant correlations concentrated mainly between 20° and 40°S but strongest between 31° and 35°S (i.e. Montecinos *et al.*, 2000a, 2000b), and negative correlations concentrated between 45° and 55°S (Figure 13(d)). The relationship between spring anomalies and $PC1_{Spring}$ proved to be significant in Central Chile, and also (but to a lesser extent) for some rain gauges located in the Northern (~20°S) and Southern regions (~53°S) (Figure 13(d)).

3.7. Gridded fields and leading modes of precipitation

Gridded data sets from the NOAA Earth System Research Laboratory were additionally used to compare and associate our previous results. [The gridded data sets are: (1) University of Delaware monthly precipitation (V3.01), 0.5° × 0.5° (latitude/longitude grid) provided by the NOAA/OAR/ESRL PSD. (2) Monthly U-winds (850 hPa) and monthly sea level pressure (SLP), 2.5° × 2.5°, provided by NCEP/NCAR Reanalysis (see Kalnay *et al.*, 1996). (3) Monthly sea surface temperature (COBE-SST2) data, 1.0° × 1.0°, provided by the NOAA/OAR/ESRL PSD (see Hirahara *et al.*, 2014).] In this regard, the leading modes of precipitation in the

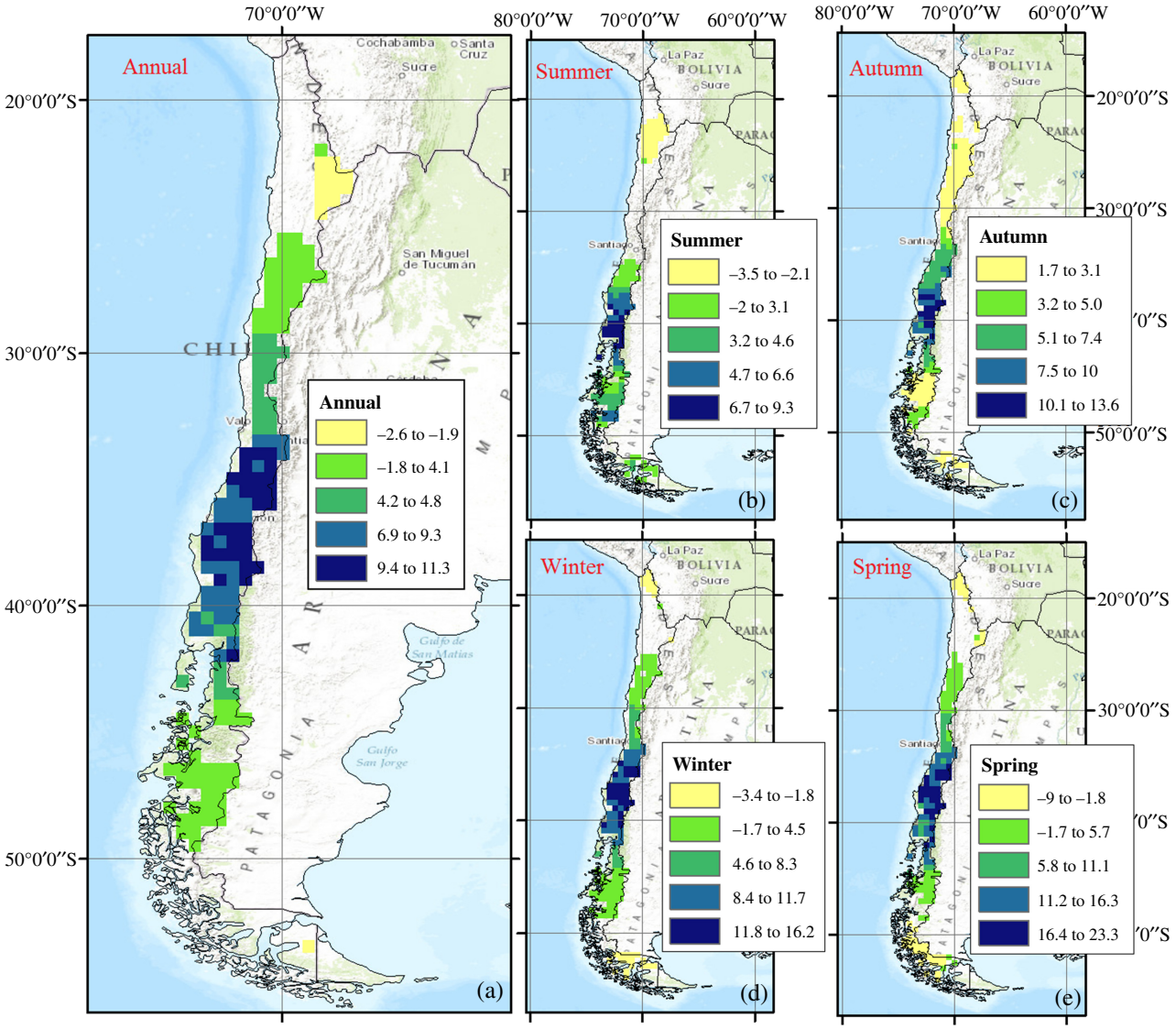

Figure 14. Significant correlation maps calculated using *t*-test, between $PC1_{Annual}$, $PC1_{Seasonal}$, and the precipitation anomalies.

Chilean domain (15°–60°S and 65°–80°W) denoted similar spatial patterns to those observed for the rain gauges, but not at all scales. For instance, the strongest significant correlations between annual precipitation anomalies and the $PC1_{Annual}$, $PC1_{Winter}$, and $PC1_{Spring}$ were concentrated between 35° and 40°S (Figure 14(a), (d), and (e)). During austral summer, there is a southward displacement of this pattern (to about 40°S), that is not so evident at the rain gauge-scale; it is probably related to the strengthening of SEPA, which blocks the passing of frontal storms in more northern locations (Figure 14(b) and (c)).

Examining the relation between PC1 and gridded fields of zonal winds at 850 hPa, SLP and SST revealed that high correlations are mostly restricted to Southern South America and the adjacent Pacific Ocean (Figure 14); however, substantial differences between summer and winter seasons are also evident. For instance, there are strong opposite correlations in different zonally elongated bands of U-winds and SLP extending across South America which are noticeable at an annual scale (Figure 14, upper maps). These bands denote a spatial pattern of U-winds that is (strongly) negatively correlated in central and southern Chile during austral winter, but positively correlated during austral summer (Figure 15, left maps). Similar patterns are observed for the seasonality of SLP and SST (Figure 15, middle and right maps), which also exhibit opposite correlations between mid- and high latitudes of Chile. This confirms that precipitation variability is clearly associated with pressure and temperature changes over the equatorial and austral Pacific Basin that can also be observed at interannual and seasonal scales. These results are in agreement with those obtained by Garreaud *et al.* (2013), who showed that the leading mode of the 850-hPa zonal winds calculated for Southern South America (35°–65°S, 90°–60°W) indicates two zonal bands spanning the whole Southern Hemisphere (SH). The results of this analysis demonstrate that the use of gridded data is an effective means of analysing climatic patterns in Chile; however, the complex geography of the country still

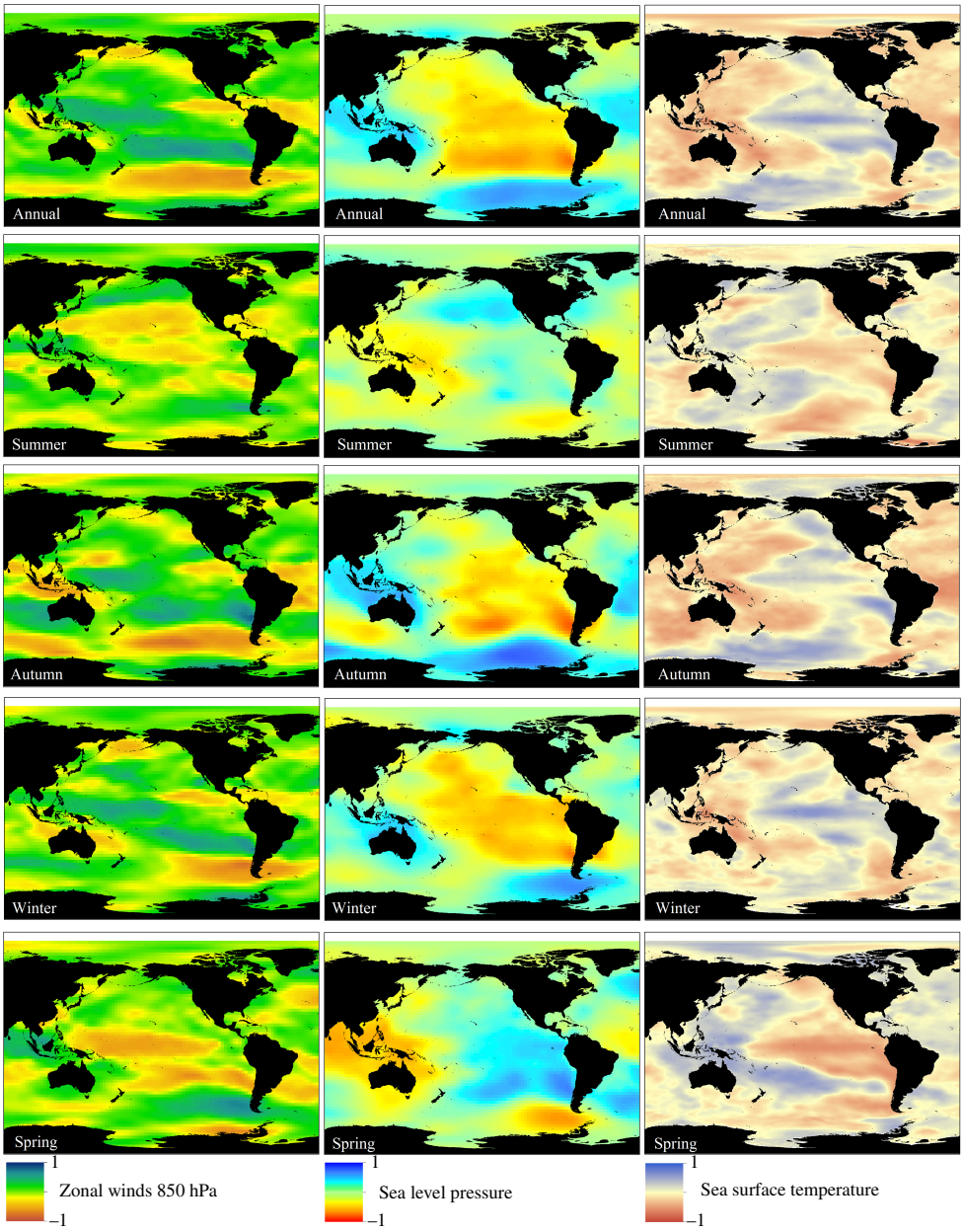

Figure 15. Leading modes of interannual ($PC1_{Annual}$) and seasonal ($PC1_{Seasonal}$) precipitation variability in Chile, projected onto the global U-winds (left maps), sea level pressure (middle maps), and sea surface temperature fields (right maps).

requires high-resolution products that can both address the narrow distances from the Andes to the Pacific Ocean and record information over the extreme South regions of the country.

3.8. Climate indices and leading modes of precipitation

Analysing the ability of each seasonally aggregated coupled ocean–atmosphere index to predict precipitation variability, it is evident that the $PC1_{Annual}$ variability is best explained by ENSO indices, especially by the negative phases (El Niño years) of the winter SOI (SOI_{Winter}) ($r = -0.61$), and even more so ($r = 0.66$) by the phases of winter Bivariate ENSO Index ($BEST_{Winter}$) (Figure 16(a) and (b)). Despite this, other ENSO indices also show significant correlations with the precipitation amounts, i.e. the mean annual values of MEI as reported by Garreaud *et al.* (2009). The phases of seasonally aggregated MJO are strongly correlated to $PC1_{Annual}$, but this relationship is not as strong as that observed for ENSO Indices. In general, the best relationships between climate indices and $PC1_{Annual}$ were observed for the winter season (same year); the exceptions are those indexes related to MJO, which showed significant correlation with summer (same year) and spring seasons (1-year back) (Table 1).

The significant modes of austral summer and spring precipitation ($PC1_{Summer}$ and $PC1_{Spring}$) were shown to be primarily related to the phases of the seasonally aggregated MJO (spring MJO8 and winter MJO6) (Figure 16(c) and (f)). The autumn mode of precipitation ($PC1_{Autumn}$) was best explained by the phases of the AAO_{Autumn}

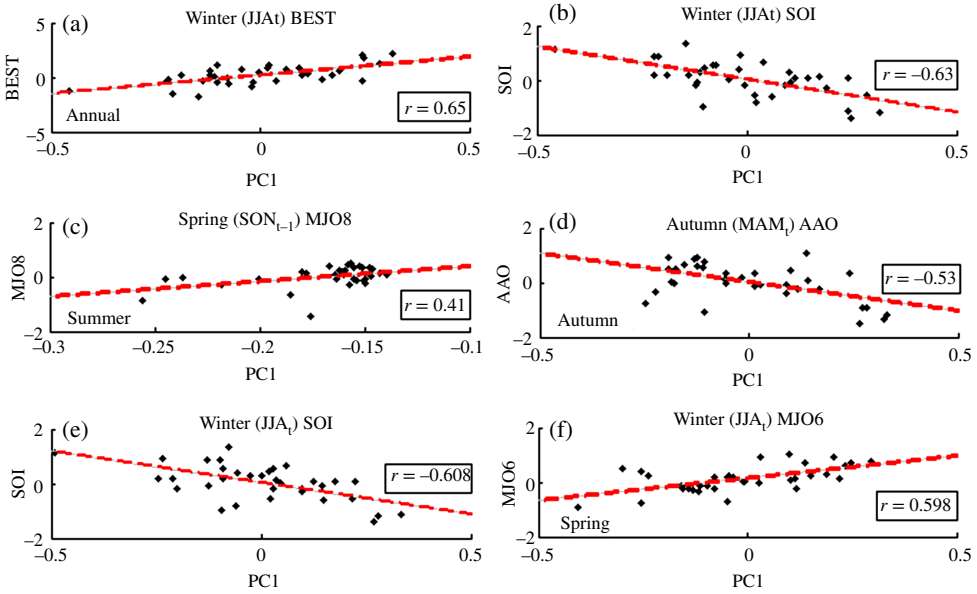

Figure 16. Scatter plots for the best correlations between different climate indices and the first significant mode of annual and seasonal precipitation ($PC1_{Annual}$ and $PC1_{Seasonal}$). Significant correlations were obtained from t-test with a critical region equal to $t(n-2;\ \alpha=0.05)=\pm 2.037$ for $n=34$ years with two degrees of freedom.

($r=-0.53$) (Figure 16(d)). Finally, the first significant mode of winter precipitation ($PC1_{Winter}$) depicted similar patterns to those observed at an annual scale, because it was mainly linked to the negative phases of the SOI_{Winter} ($r=-0.61$) (Figure 16(e)). A summary of the results obtained for each significant mode of annual and seasonal precipitation (PC1, PC2, and PC3), and the climate indices used in this study are presented in Table 2.

4. Discussion

4.1. Leading modes of precipitation and ocean–atmosphere teleconnections

The changes in the annual and seasonal rainfall regimes in Chile were described in the context of the evolution of major regional and large-scale factors controlling rainfall variability along the extratropical west coast of South America. The PCA method was used to describe and analyse the main significant modes of annual and seasonal precipitation variability in Chile, and to reveal the influence of different climate indices and gridded ocean–atmospheric fields. In general, the approach showed that the explained variance of the first significant modes of annual and seasonal precipitation ranged between 43% during spring ($PC1_{Spring}$) and 55% at an annual scale ($PC1_{Annual}$). Additionally, the explained variance of second significant mode of precipitation ranged between 13.6% in the fall ($PC2_{Autumn}$) and 20% in the summer ($PC2_{Summer}$). Regarding annual and spring precipitation patterns, no significant correlations were observed for PC2. Finally, the explained variance of third significant mode of precipitation ranged between 6.3% in winter ($PC3_{Winter}$) and 8.7% in austral summer ($PC3_{Summer}$); again the annual and spring precipitation patterns were not observed to be significant. The observed spatial (point-based) precipitation patterns were concentrated in Central Chile, especially for the first leading modes of annual and seasonal precipitation. The precipitation patterns in the Northern and Southern regions of Chile were mainly explained by the second and third leading modes (PC2 and PC3) of annual and seasonal precipitation. The use of gridded data at global scale denoted several spatial patterns extending across South America (U-winds, SLP, and SST), which are noticeable at an annual and seasonal scale. In this context, precipitation variability is clearly associated with pressure and temperature changes over the equatorial and austral Pacific Basin that can clearly be observed at an interannual scale (Garreaud *et al.*, 2013), but also at a seasonal scale.

The use of climatic indices revealed that the SOI_{Winter} explained most of the interannual and winter variability of precipitation (see also Rutllant and Fuenzalida, 1991; Aceituno and Garreaud, 1995; Garreaud and Batisti, 1999; Montecinos and Aceituno, 2003; Garreaud *et al.*, 2009). The immediate effects of ENSO modulation in the variability of precipitation can be explained by the propagation of Rossby waves caused by heat anomalies in the tropical central Pacific that modify the normal atmospheric circulation, generating changes in the storm track that impact Chile (Pizarro *et al.*, 2002). The close relationship between winter and annual accumulation is in agreement with the results of SR_I for central Chile, because in the subtropical domain along the West coast of the continent between 40 and 80% of precipitation falls during the austral winter. This phenomenon is primarily associated with extratropical systems that reach this region when the subtropical anticyclone in the southeast Pacific and the mid-latitude band of migratory low pressure systems are

Table 2. Summary of the results obtained for the leading modes of annual/seasonal precipitation variability in Chile, and their relationships to precipitation anomalies and seasonally aggregated climate indices.

Anomalies	Pattern	Significant (leading) modes of annual or seasonal precipitation		
		PC_1	PC_2	PC_3
Annual	Anomalies	$PC1_{Annual}$ explained 55.3% of variance with significant correlations between 20° and 40°S; however, the most substantial spatial pattern of SMP-annual was found to be mainly concentrated in central Chile (30°–40°S).	$PC2_{Annual}$ explained 9.3% of variance however the mode is not significant.	$PC3_{Annual}$ explained 7.9% of variance however the mode is not significant.
	Climate indices	Winter SOI (negative phase) and BEST (positive phase) indices corresponding to the same year (JJA_t), with a strong and significant spatial influence mainly concentrated in central Chile (30°–35°S).	No significant mode was observed. Therefore, no correlations with climatic indices were calculated.	No significant mode was observed. Therefore, no correlations with climatic indices were calculated.
DJF (summer)	Anomalies	$PC1_{Summer}$ explained 46% of variance with mostly negative and significant correlations between 30° and 40°S.	$PC2_{Summer}$ explained 20% of variance with similar results to the first mode; however, this time the spatially significant influence was mainly observed between 33° and 40°S.	$PC3_{Summer}$ explained 8.7% of variance, and it was significantly correlated in northern regions above 25°S.
	Climate indices	Spring MJO (phases 7 and 8) (SON_t) was related to the First SMP-DJF, especially significant in regions 35°S northward.	Summer PDO (positive phase) (DJF_t) proved to be the exclusive pattern significantly correlated with both the second SMP-DJF and DJF anomalies for the region between 33° and 40°S.	Spring N3.4 (negative phase) (SON_{t-1}) was associated with the third SMP-DJF mainly observed over northern regions between 17° and 25°S. Also some spatial influence was detected around 33°S.
MAM (autumn)	Anomalies	$PC1_{Autumn}$ explained 51% of variance, and it showed mostly positive and significant correlations between 30° and 40°S with the strongest activity around 35°S.	$PC2_{Autumn}$ explained 13.6% of variance. Significant correlations were observed as a meridional dipole, with positive values between 30° and 33°S, and negative values between 38° and 40°S.	$PC3_{Autumn}$ explained 6.5% of variance. It also showed a dipole pattern strongly marked in northern Chile (about 25°S northward and with some significances observed about 45°S and south of 50°S as well.
	Climate indices	Autumn activity (MAM_t) of the same year for the Antarctic Oscillation Index (AAO) (negative phase). Significant spatial influence was distributed from 30° to 40°S with the largest values observed between 35° and 40°S.	Spring AAO (negative phases) of the previous season (SON_{t-1}), was significantly correlated with the second SMP-MAM, influencing the MMA precipitation pattern specifically between 30° and 35°S.	Autumn MJO7 Index (phase 7, positive) of the same season (MAM_t) was found to be significantly correlated with the Third SMP-MAM. The spatial influence is specifically concentrated over regions located 25°S northward.

Table 2. continued

Anomalies	Pattern	Significant (leading) modes of annual or seasonal precipitation		
		PC_1	PC_2	PC_3
JJA (winter)	Anomalies	$PC1_{Winter}$ explained 52.3% of variance in the area between 27° and 40°S.	$PC2_{Winter}$ explained 14.5% of variance. A dipole pattern was observed to be positive around 32°S and negative around 37°S.	$PC3_{Winter}$ explained 6.3% of variance. It showed to be significantly correlated to those stations located in regions 25°S northward.
	Climate indices	Winter SOI (negative phase) and BEST (positive phase) indices corresponded to the same season (JJA_t), with a strong and significant spatial influence mainly concentrated in central Chile (30°–35°S).	Autumn AAO (negative phase) of the previous season (MAM_{t-1}). The spatial dipole was not entirely defined by the pattern. Only those stations located about 37° and 40°S showed significant correlations.	Autumn N3.4 (negative phase) of the previous season (MAM_{t-1}). It showed significant influence over northern regions above 25°S.
SON (spring)	Anomalies	$PC1_{Spring}$ explained 43% of variance and showed significant correlations for central Chile between 30° and 40°S, and strongly correlated around 35°S.	$PC2_{Spring}$ explained 16.7% of variance; however, the mode is not significant.	$PC3_{Spring}$ explained 14.4% of variance; however, the mode is not significant.
	Climate indices	Winter MJO6 (phase 6, positive) strongly correlated to those stations located between 35° and 40°S.	No significant mode was observed. Therefore, no correlations against climatic indices were carried out.	No significant mode was observed. Therefore, no correlations against climatic indices were carried out.

at their northernmost position (Montecinos and Aceituno, 2003; Garreaud *et al.*, 2009).

The AAO_{Autumn} was found to be the main source of autumn precipitation variability in Central Chile. The AAO plays a significant role in modulating the interannual rainfall variability in all of central Chile, especially during the austral winter semester (April–September). This is because this pattern is partially connected to changes in the meridional SLP gradient at mid- and high latitudes in the southeast Pacific (Quintana and Aceituno, 2012). Villalba *et al.* (2012) mentioned that negative (positive) precipitation anomalies in northern Patagonia (38°–42°S) are related to positive (negative) phases of the AAO. Moreover, no significant results were observed for the AAO in the southern regions (south of 45°S). This is probably due to the lack of point-based data in the intermediate regions (40° and 50°S), which may be an important source of possible misleading results.

The MJO_{Spring} explained most of the summer precipitation variability (phases 7 and 8), and also most of the spring variability (phase 6). In a composites analysis of precipitation and rainfall intensity in Central-South Chile (30°–45°S) in relation to the real-time multivariate MJO index, Barrett *et al.* (2012) showed that above normal precipitation and greater frequency of heavy precipitation occurred during phases 8, 1, and 2; the study also showed that below normal precipitation takes place in phases 3–7. In other words, when the deep convective clouds and rainfall are located in the Pacific Basin, the atmospheric circulation can demonstrate an ENSO-like pattern. Therefore, during this phase, precipitation and heavy rainfall events are more likely to occur in the extratropical region, such as the Chilean territory facing the southeastern Pacific Ocean (Carrasco, 2006; Barrett *et al.*, 2012).

5. Conclusions

Because Chile's regions span from subtropical to extratropical latitudes, there is a strong latitudinal influence in precipitation accumulation which is observed at both annual and seasonal scales. In addition, a narrow distance between the Pacific Ocean and the Andes Mountain range depict an important orographic effect which depends on local orographic conditions and the source of precipitation. In general, Northern regions are affected by rain shadow conditions in the western Andean slopes; however, Central regions can denote important ER in the cross-mountain direction. Southern regions receive large contribution of precipitation from westerlies that generate rain shadow conditions in the eastern Andean slopes.

The SR_I showed that most of the contribution of seasonal precipitation to annual accumulation occurs in Central Chile, especially for winter accumulation. This situation was completely different in Northern Chile where most of the annual precipitation is contributed by summer accumulation. We also found significant evidence of temporal changes in the SR_I during autumn and winter seasons.

These trends are exclusively concentrated in central and southern regions of Chile.

According to our results, the SPI can satisfactorily explain the intensity of droughts in Chile. However, it is not a valid index in arid regions, such as those regions located above 25°S (Atacama Desert) in Northern Chile, where precipitation often varies from zero to several inches over relatively short periods. The probability analysis demonstrated that, primarily for central Chile, very dry and extremely dry conditions are more likely during La Niña years. On the other hand, very wet and extremely wet conditions were mostly observed during El Niño years.

The annual and seasonal rainfall variability is mostly explained by the first leading mode of precipitation (PC1), especially for Central Chile. The second and third modes of precipitation were found to be significant only for autumn, winter, and spring accumulation. The leading modes of annual/winter precipitation deployed significant relationships with SOI_{Winter}, confirming that most of the interannual and winter precipitation variability in Chile can be explained by ENSO phenomena. Significant relationships also were found between seasonally aggregated MJO indices and spring/summer precipitation. This suggests that the seasonal spring/summer precipitation variability in central Chile could be satisfactorily predicted with seasonally averaged MJO indices, especially using phases 6, 7, and 8. Finally, fall precipitation was better explained by the fall AAO, demonstrating that this low-frequency variability mode (in its aggregated version) also accounts for part of the seasonal precipitation in central Chile. The significant spatial patterns of these relationships are in concordance with the analysis of gridded data based on U-winds, SLP, and SST.

The ocean–atmospheric processes that affect precipitation variability in Chile are very complex because there are several factors that influence seasonal and annual accumulation. Despite the detailed annual and seasonal analysis conducted here, more detailed country-based studies are still required to develop a comprehensive understanding of the climatic patterns in a country which is geographically very difficult to study. For example, future studies will be required to define how ocean–atmosphere processes affect the spatio-temporal variability of precipitation accumulation at a monthly or daily scale; and also determine how global warming will disturb the future availability and distribution of water resources in Chile.

Acknowledgements

The support of the *Dirección General de Aguas* (DGA) of Chile is greatly acknowledged because it provided all of the rainfall data to conduct this study.

Supporting Information

The following supporting information is available as part of the online article:
Appendix S1. Supplementary Optional Material.

References

Aceituno P, Garreaud R. 1995. Impacto de los fenómenos el Niño y la Niña en el régimen pluviométrico Andino. *Revista Chilena de Ingeniería Hidráulica* **9**: 12–20.

Allen MJ, Sheridan SC. 2015. Evaluating changes in season length, onset, and end dates across the United States (1948–2012). *Int. J. Climatol.* , doi: 10.1002/joc.4422.

Ancapichún S, Garcés-Vargas J. 2015. Variability of the southeast Pacific subtropical anticyclone and its impact on sea surface temperature off north-central Chile. *Cienc. Mar.* **41**(1): 1–20.

Andrews DG, Holton JR, Leovy CB. 2003. Inter tropical convergence zones. *Atmos. Sci.* **56**: 374–399.

Aravena JC, Luckman BH. 2009. Spatio-temporal rainfall patterns in Southern South America. *Int. J. Climatol.* **29**(14): 2106–2120, doi: 10.1002/joc.1761.

Archer CL, Caldeira K. 2008. Historical trends in the jet streams. *Geophys. Res. Lett.* **35**: L08803, doi: 10.1029/2008GL033614.

Barrett BS, Carrasco JF, Testino AP. 2012. Madden-Julian oscillation (MJO) modulation of atmospheric circulation and Chilean winter precipitation. *J. Clim.* **25**: 1678–1688.

Bazrafshan J, Hejabi S, Rahimi J. 2014. Drought monitoring using the multivariate standardized precipitation index (MSPI). *Water Resour. Manage.* **28**(4): 1045–1060, doi: 10.1007/s11269-014-0533-2.

Beguería S, Vicente-Serrano SM, Reig F, Latorre B. 2014. Standardized precipitation evapotranspiration index (SPEI) revisited: parameter fitting, evapotranspiration models, tools, datasets and drought monitoring. *Int. J. Climatol.* **34**: 3001–3023, doi: 10.1002/joc.3887.

Bombardi RJ, Carvalho LM, Jones C, Reboita MS. 2014. Precipitation over eastern South America and the South Atlantic Sea surface temperature during neutral ENSO periods. *Clim. Dyn.* **42**(5–6): 1553–1568.

Bonaccorso B, Cancelliere A, Rossi G. 2015. Probabilistic forecasting of drought class transitions in Sicily (Italy) using Standardized Precipitation Index and North Atlantic Oscillation Index. *J. Hydrol.* **526**: 136–150.

Carrasco J. 2006. Precipitation events in Central Chile and its relation with the MJO. In *Proceedings of 8th ICSHMO*, INPE, Foz do Iguaçu, Brazil, 24–28 April 2006, 1719–1722.

Carrasco JF, Casassa G, Rivera A. 2002. Meteorological and climatological aspects of the Southern Patagonia Icefield. In *The Patagonian Icefields: Unique Natural Laboratory for Environmental and Climate Change Studies*, Casassa G, Sepúlveda F, Sinclair R (eds). Kluwer Academic/Plenum Publishers: New York, NY, 29–41.

Carrasco JF, Osorio R, Casassa G. 2008. Secular trend of the equilibrium-line altitude on the western side of the southern Andes, derived from radiosonde and surface observations. *J. Glaciol.* **54**(186): 538–550.

Carvalho LM, Jones C, Posadas AN, Quiroz R, Bookhagen B, Liebmann B. 2012. Precipitation characteristics of the South American monsoon system derived from multiple datasets. *J. Clim.* **25**(13): 4600–4620.

Falvey M, Garreaud R. 2007. Wintertime precipitation episodes in Central Chile: associated meteorological conditions and orographic influences. *J. Hydrometeorol.* **8**(2): 171–193.

Fix E, Hodges JL. 1989. An important contribution to nonparametric discriminant analysis and density estimation. Commentary on Fix and Hodges. 1951. B. W. Silverman and M. C. Jones. *Int. Stat. Rev./Revue Internationale de Statistique* **57**(3): 233–238.

Fuenzalida HP, Ruttlant J. 1987. Origen del vapor de agua que precipita sobre el Altiplano de Chile. In *Proceeding of II Congreso Inter-Americano de Meteorologia*, American Meteorological Society, Buenos Aires, 6.3.1–6.3.4.

Garreaud R. 1999. Multiscale analysis of the summertime precipitation over the central Andes. *Mon. Weather Rev.* **127**: 901–921, doi: 10.1175/1520-0493(1999)127<0901:MAOTSP>2.0.CO;2.

Garreaud R. 2000. Intraseasonal variability of moisture and rainfall over the South American Altiplano. *Mon. Weather Rev.* **128**(9): 3337–3346.

Garreaud R, Aceituno P. 2001. Interannual rainfall variability over the South American Altiplano. *J. Clim.* **14**: 2779–2789, doi: 10.1175/1520-0442(2001)014<2779:IRVOTS>2.0.CO;2.

Garreaud RD, Aceituno P. 2007. Atmospheric circulation over South America: mean features and variability. In *The Physical Geography of South America*, Veblen T, Young K, Orme A (eds). Oxford University Press: Oxford, UK, 45–59.

Garreaud R, Batisti D. 1999. Inter-annual (ENSO) and inter-decadal (ENSO-like) variability of the Southern Hemisphere tropospheric circulation. *J. Clim.* **12**: 2113–2123.

Garreaud RD, Wallace JM. 1997. The diurnal march of the convective cloudiness over the Americas. *Mon. Weather Rev.* **125**: 3157–3171.

Garreaud RD, Wallace JM. 1998. Summertime incursions of mid-latitude air into tropical and subtropical South America. *Mon. Weather Rev.* **126**: 2713–2733.

Garreaud R, Vuille M, Clement AC. 2003. The climate of the Altiplano: observed current conditions and mechanisms of past changes. *Palaeogeogr. Palaeoclimatol. Palaeoecol.* **194**(1): 5–22.

Garreaud R, Vuille M, Compagnucci R, Marengo J. 2009. Present-day South American climate. *Palaeogeogr. Palaeoclimatol. Palaeoecol.* **281**(3–4): 180–195, doi: 10.1016/j.palaeo.2007.10.032.

Garreaud R, Lopez P, Minvielle M, Rojas M. 2013. Large-scale control on the Patagonian climate. *J. Clim.* **26**(1): 215–230.

Garreaud RD, Gabriela Nicora M, Bürgesser RE, Ávila EE. 2014. Lightning in western Patagonia. *J. Geophys. Res. Atmos.* **119**(8): 4471–4485.

Guttman NB. 1998. Comparing the Palmer drought index and the Standardized Precipitation Index. *J. Am. Water Resour. Assoc.* **34**(1): 113–121, doi: 10.1111/j.1752-1688.1998.tb05964.x.

Hartmann DL, Klein Tank AMG, Rusticucci M, Alexander LV, Brönnimann S, Charabi Y, Dentener FJ, Dlugokencky EJ, Easterling DR, Kaplan A, Soden BJ, Thorne PW, Wild M, Zhai PM. 2013. Observations: atmosphere and surface. In *Climate Change 2013: The Physical Science Basis. Contribution of Working Group I to the Fifth Assessment Report of the Intergovernmental Panel on Climate Change*, Stocker TF, Qin D, Plattner G-K, Tignor M, Allen SK, Boschung J, Nauels A, Xia Y, Bex V, Midgley PM (eds). Cambridge University Press: Cambridge, UK and New York, NY.

Hirahara S, Ishii M, Fukuda Y. 2014. Centennial-scale sea surface temperature analysis and its uncertainty. *J. Clim.* **27**: 57–75, doi: 10.1175/JCLI-D-12-00837.1.

Horel JD, Hahmann AN, Geisler JE. 1989. An investigation of the annual cycle of convective activity over the tropical Americas. *J. Clim.* **2**: 1388–1403.

Houston J. 2006. Variability of precipitation in the Atacama Desert: its causes and hydrological impact. *Int. J. Climatol.* **26**: 2181–2198, doi: 10.1002/joc.1359.

Houston J, Hartley AJ. 2003. The central Andean west-slope rain shadow and its potential contribution to the origin of hyper-aridity in the Atacama Desert. *Int. J. Climatol.* **23**(12): 1453–1464.

IPCC. 2012. Summary for policymakers. In *Managing the Risks of Extreme Events and Disasters to Advance Climate Change Adaptation. A Special Report of Working Groups I and II of the Intergovernmental Panel on Climate Change*, Field CB, Barros V, Stocker TF, Qin D, Dokken DJ, Ebi KL, Mastrandrea MD, Mach KJ, Plattner G-K, Allen SK, Tignor M, Midgley PM (eds). Cambridge University Press: Cambridge, UK, and New York, NY, 3–21.

Jolliffe IT. 2002. *Principal Component Analysis Series*. Springer Series in Statistics, Vol. XXIX, 487 pp, 2nd edn. Springer: New York, NY. ISBN: 978-0-387-95442-4.

Kalnay E, Kanamitsu M, Kistler R, Collins W, Deaven D, Gandin L, Iredell M, Saha S, White G, Woollen J, Zhu Y, Chelliah M, Ebisuzaki W, Higgins W, Janowiak J, Mo K, Ropelewski C, Wang J, Leetmaa A, Reynolds R, Jenne R, Joseph D. 1996. The NCEP/NCAR 40-year reanalysis project. *Bull. Am. Meteorol. Soc*. **77**(3): 437–471.

Karavitis C, Alexandris S, Tsesmelis D, Athanasopoulos G. 2011. Application of the Standardized Precipitation Index (SPI) in Greece. *Water* **3**: 787–805, doi: 10.3390/w3030787.

Keyantash J, Dracup JA. 2002. The quantification of drought: an evaluation of drought indices. *Bull. Am. Meteorol. Soc.* **83**: 1167–1180.

Madden R, Julian P. 1971. Detection of a 40-50 day oscillation in the zonal wind in the tropical Pacific. *J. Atmos. Sci.* **28**: 702–708.

Madden R, Julian P. 1972. Description of global-scale circulation cells in the tropics with a 40-50 day period. *J. Atmos. Sci.* **29**: 1109–1123.

Marengo JA, Liebmann B, Kousky VE, Filizola NP, Wainer IC. 2001. Onset and end of the rainy season in the Brazilian Amazon Basin. *J. Clim.* **14**(5): 833–852.

Marengo JA, Liebmann B, Grimm AM, Misra V, Silva Dias PL, Cavalcanti IFA, Carvalho LMV, Berbery EH, Ambrizzi T, Vera CS, Saulo AC, Nogues-Paegle J, Zipser E, Seth A, Alves LM. 2012. Recent developments on the South American monsoon system. *Int. J. Climatol.* **32**(1): 1–21.

Marshall J, Donohoe A, Ferreira D, McGee D. 2014. The ocean's role in setting the mean position of the inter-tropical convergence zone. *Clim. Dyn.* **42**(7–8): 1967–1979.

McKee TB, Doesken NJ, Kleist J. 1993. The relationship of drought frequency and duration of time scales. In *Eighth Conference on Applied Climatology*, American Meteorological Society, Anaheim CA, 17–23 January 1993, 179–186.

Meinke H, deVoil P, Hammer GL, Power S, Allan R, Stone RC, Folland C, Potgieter A. 2005. Rainfall variability at decadal and longer time scales: signal or noise? *J. Clim.* **18**: 89–96, doi: 10.1175/JCLI-3263.1.

Meza FJ. 2013. Recent trends and ENSO influence on droughts in Northern Chile: an application of the Standardized Precipitation Evapotranspiration Index. *Weather Clim. Extremes* **1**: 51–58.

Minvielle M, Garreaud RD. 2011. Projecting rainfall changes over the South American Altiplano. *J. Clim.* **24**(17): 4577–4583.

Montecinos A, Aceituno P. 2003. Seasonality of the ENSO-related rainfall variability in central Chile and associated circulation anomalies. *J. Clim.* **16**: 281–296.

Montecinos A, Díaz A, Aceituno P. 2000a. Seasonal diagnostic and predictability of rainfall in subtropical South America based on tropical Pacific SST. *J. Clim.* **13**: 746–758.

Montecinos A, Garreaud R, Aceituno P. 2000b. Interdecadal rainfall variability in subtropical South America and its relationship with tropical Pacific SST. In *6th International Conference on Southern Hemisphere Meteorology and Oceanography*, Santiago, 3–7 April 2000, 67–68.

Montecinos A, Kurgansky M, Muñoz C, Takahashi K. 2011. Non-ENSO interannual rainfall variability in central Chile during austral winter. *Theor. Appl. Climatol.* **106**(3–4): 557–568, doi: 10.1007/s00704-011-0457-1.

Mwangi E, Wetterhall F, Dutra E, Di Giuseppe F, Pappenberger F. 2014. Forecasting droughts in East Africa. *Hydrol. Earth Syst. Sci.* **18**: 611–620, doi: 10.5194/hess-18-611-2014.

North GR, Bell TL, Cahalan RF, Moeng FJ. 1982. Sampling errors in the estimation of empirical orthogonal functions. *Mon. Weather Rev.* **110**(7): 699–706.

Núñez JH, Verbist K, Wallis JR, Schaefer MG, Morales L, Cornelis WM. 2011. Regional frequency analysis for mapping drought events in north-central Chile. *J. Hydrol.* **405**(3): 352–366.

Núñez J, Rivera D, Oyarzún R, Arumí JL. 2014. On the use of Standardized Drought Indices under decadal climate variability: critical assessment and drought policy implications. *J. Hydrol.* **517**: 458–470.

Pezoa LS. 2003. *Compilation and Analysis of Temperature (1965–2001) and Precipitation (1931–2001) Variations from the Information of Meteorological Stations in Chile between 33° and 53°S*. Forest Engineer thesis, Universidad Austral de Chile, Valdivia, Chile.

Pizarro O, Shaffer G, Dewitte B, Ramos M. 2002. Dynamics of seasonal and interannual variability of the Peru-Chile undercurrent. *Geophys. Res. Lett.* **29**(12): 22–1.

Pizarro R, Valdés R, García-Chevesich P, Vallejos C, Sangüesa C, Morales C, Balocchi F, Abarza A, Fuentes R. 2012. Latitudinal analysis of rainfall intensity and mean annual precipitation in Chile. *Chilean J. Agric. Res.* **72**(2): 252–261.

Quintana J, Aceituno P. 2012. Changes in the rainfall regime along the extratropical west coast of South America (Chile): 30 – 43°S. *Atmósfera* **25**(1): 1–22.

Rahn D, Garreaud R. 2014. A synoptic climatology of the near-surface wind along the west coast of South America. *Int. J. Climatol.* **34**: 780–792, doi: 10.1002/joc.3724.

Rutllant J, Fuenzalida H. 1991. Synoptic aspects of the Central Chile rainfall variability associated with the Southern Oscillation. *Int. J. Climatol.* **11**: 63–76.

Spath H. 1985. *Cluster Dissection and Analysis: Theory, FORTRAN Programs, Examples (Translated by J. Goldschmidt)*. Halsted Press: New York, NY.

Trenberth KE, Jones PD, Ambenje P, Bojariu R, Easterling D, Tank AK, Parker D, Rahimzadeh F, Renwick JA, Rusticucci M, Soden B, Zhai P. 2007. Observations: surface and atmospheric climate change. In *Climate Change 2007: The Physical Science Basis. Contribution of Working Group I to the Fourth Assessment Report of the Intergovernmental Panel on Climate Change*, Solomon S, Qin D, Manning M, Chen Z, Marquis M, Averyt KB, Tignor M, Miller HL (eds). Cambridge University Press: Cambridge, UK, 235–336.

Valdés-Pineda R, Pizarro R, García-Chevesich P, Valdés JB, Olivares C, Vera M, Balocchi F, Perez F, Vallejos C, Fuentes R, Abarza A, Helwig B. 2014. Water governance in Chile: availability, management and climate change. *J. Hydrol.* **519**: 2538–2567, doi: 10.1016/j.jhydrol.2014.04.016.

Valdés-Pineda R, Pizarro R, Valdés JB, Carrasco JF, García-Chevesich P, Olivares C. 2015. Spatio-temporal trends of precipitation, its aggressiveness and concentration, along the Pacific coast of South America (36°–49° S). *Hydrol. Sci. J.* (in press).

Vargas G, Ortlieb L, Rutllant J. 2000. Aluviones históricos en Antofagasta y su relación con eventos El Niño/Oscilación del Sur. *Rev. geol. Chile* **27**(2): 157–176.

Vargas G, Pantoja S, Rutllant JA, Lange CB, Ortlieb L. 2007. Enhancement of coastal upwelling and interdecadal ENSO-like variability in the Peru-Chile Current since late 19th century. *Geophys. Res. Lett.* **34**: L13607, doi: 10.1029/2006GL028812.

Vera C, Higgins W, Amador J, Ambrizzi T, Garreaud R, Gochis D, Gutzler D, Lettenmaier D, Marengo J, Mechoso CR, Nogues-Paegle J, Silva Dias PL, Zhang C. 2006. Toward a unified view of the American monsoon systems. *J. Clim.* **19**(20): 4977–5000.

Verbist K, Robertson AW, Cornelis WM, Gabriels D. 2010. Seasonal predictability of daily rainfall characteristics in Central Northern Chile for dry-land management. *J. Appl. Meteorol. Climatol.* **49**: 1938–1955, doi: 10.1175/2010JAMC2372.1.

Viale M, Garreaud R. 2015. Orographic effects of the subtropical and extratropical Andes on upwind precipitating clouds. *J. Geophys. Res. Atmos.* **120**: 4962–4974, doi: 10.1002/2014JD023014.

Vicente-Serrano SM, Gonzalez-Hidalgo JC, de Luis M, Raventos J. 2004. Drought patterns in the Mediterranean area: the Valencia region (eastern Spain). *Clim. Res.* **26**: 5–15.

Vicente-Serrano S, Beguería S, López-Moreno JI. 2010. A multiscalar drought index sensitive to global warming: the standardized precipitation evapotranspiration index. *J. Clim.* **23**: 1696–1718, doi: 10.1175/2009JCLI2909.1.

Villalba R, Lara A, Masiokas MH, Urrutia RB, Luckman BH, Marshall GJ, Mundo IA, Christie DA, Cook ER, Neukom R, Allen K, Fenwick P, Boninsegna JA, Srur AM, Morales MS, Araneo D, Palmer JG, Cuq E, Aravena JC, Holz A, Le Quesne C. 2012. Unusual Southern Hemisphere tree growth patterns induced by changes in the Southern Annular Mode. *Nat. Geosci.* **5**: 793–798.

Villarroel C. 2013. *Eventos extremos de precipitación y temperatura en Chile: proyecciones para fines del siglo XXI*. http://www.repositorio.uchile.cl/handle/2250/114066 (accessed 29 June 2015).

Vuille M. 1999. Atmospheric circulation over the Bolivian Altiplano during dry and wet periods and extreme phases of the Southern Oscillation. *Int. J. Climatol.* **19**: 1579–1600, doi: 10.1002/(SICI)1097-0088(19991130)19:14<1579::AID-JOC441>3.0.CO;2-N.

Vuille M, Hardy DR, Braun C, Keimig F, Bradley RS. 1998. Atmospheric circulation anomalies associated with 1996/1997 summer precipitation events on Sajama Ice Cap, Bolivia. *J. Geophys. Res.* **103**(D10): 11191–11204.

Wilhite D, Svoboda M, Hayes M. 2005. Monitoring drought in the United States: status and trends. In *Monitoring and Predicting Agricultural Drought, A Global Study*, Boken VK, Cracknell AP, Heathcote RL (eds). Oxford University Press: New York, NY, 121–131.

Wu H, Svoboda MD, Hayes MJ, Wilhite DA, Fujiang W. 2006. Appropriate application of the standardized precipitation index in arid locations and dry seasons. *Int. J. Climatol.* **27**: 65–79.

Zamboni L, Kucharski F, Mechoso CR. 2012. Seasonal variations of the links between the interannual variability of South America and the South Pacific. *Clim. Dyn.* **38**(9–10): 2115–2129, doi: 10.1007/s00382-011-1116-z.

Zarch MAA, Sivakumar B, Sharma A. 2015. Droughts in a warming climate: a global assessment of standardized precipitation index (SPI) and reconnaissance drought index (RDI). *J. Hydrol.* **526**: 183–195.

Zhang C. 2005. Madden-Julian Oscillation. *Rev. Geophys.* **43**: 1–36.

Zhou J, Lau KM. 1998. Does a monsoon climate exist over South America? *J. Clim.* **11**(5): 1020–1040.

